Leptogenesis from low energy CP violation

K. Moffat,[a] **S. Pascoli,**[a] **S.T. Petcov**[b,c] **and J. Turner**[d]

[a]*Institute for Particle Physics Phenomenology, Department of Physics,*
Durham University, South Road, Durham DH1 3LE, U.K.

[b]*SISSA/INFN,*
Via Bonomea 265, I-34136 Trieste, Italy.

[c]*Kavli IPMU (WPI), University of Tokyo,*
5-1-5 Kashiwanoha, 277-8583 Kashiwa, Japan.

[d]*Theoretical Physics Department,*
Fermi National Accelerator Laboratory, P.O. Box 500, Batavia, IL 60510, U.S.A.

E-mail: kristian.p.moffat@durham.ac.uk, silvia.pascoli@durham.ac.uk, petcov@sissa.it, jturner@fnal.gov

Abstract: We revisit the possibility of producing the observed baryon asymmetry of the Universe via thermal leptogenesis, where CP violation comes exclusively from the low-energy phases of the neutrino mixing matrix. We demonstrate the viability of thermal flavoured leptogenesis across seven orders of magnitude $\left(10^6 < T \text{ (GeV)} < 10^{13}\right)$, using modern numerical machinery, where the lower bound can be reached only if flavour effects are taken into account and its value depends on the allowed degree of cancellation between the tree-level and radiative contributions to the light neutrino masses. At very high scales $\left(T \gg 10^{12} \text{ GeV}\right)$, we clarify that thermal leptogenesis is sensitive to the low-energy phases, in contradiction with what is usually claimed in the literature. In particular we demonstrate that Majorana-phase leptogenesis is in general viable while Dirac-phase leptogenesis requires some level of fine-tuning.

Contents

1 Introduction

The Standard Model (SM) cannot explain the observed baryon asymmetry of the Universe (BAU) in spite of qualitatively satisfying the Sakharov conditions.[1] Similarly, physics beyond the SM is often invoked to explain the existence of the non-zero neutrino masses [2]. Leptogenesis is a mechanism by which some lepton-number-violating theories, which may also explain the origin of neutrino masses, produce a lepton asymmetry which is subsequently converted into a baryon asymmetry through the non-perturbative $(B+L)$-violating but $(B-L)$-conserving sphaleron processes of the SM [3, 4]. A minimal implementation of leptogenesis occurs in the type I seesaw framework in which a number of heavy Majorana neutrinos are added to the SM [5–8]. The decay of these heavy Majorana neutrinos in leptons and Higgs bosons is both lepton-number- and CP-violating and occurs out of thermal equilibrium, thereby satisfying the Sakharov conditions and potentially producing the observed baryon asymmetry [9] (see also, e.g., [10–13] and articles quoted therein). CP violation is fundamental to the creation of the matter-antimatter asymmetry. In thermal leptogenesis, the decays of the heavy Majorana neutrinos are CP-asymmetric and this results from both CP-violating low-scale measurable phases and high-scale immeasurable ones. In the original conception of leptogenesis, the flavour-dependent interactions due to charged lepton Yukawa couplings between the leptons and the early Universe plasma were disregarded. If leptogenesis occurs at high scales, where the temperature $T \gg 10^{12}$ GeV, then this approximation is ordinarily justified and a basis may be chosen in which essentially only one flavour of lepton ever appears in the theoretical description. Consequently, it was expected that the low-energy CP-violating phases contained in the neutrino mixing matrix play no physical role in the production of the lepton and therefore baryon asymmetry [11, 12].

Under certain ad hoc assumptions the high-scale CP-violating phases can be related to the CP-violating phases in the Pontecorvo-Maki Nakagawa-Sakata (PMNS) matrix (see, e.g., [14]) which then participate in the production of the lepton asymmetry — a possibility that was investigated in [15–19]. If leptogenesis occurs at temperatures somewhat below 10^{12} GeV $\left(10^9 \text{ GeV}\right)$, the Yukawa interactions of the tau charged lepton (of the muon) come into thermal equilibrium, causing decoherence between this and the remaining flavour components of the charged lepton state [20–24] such that two (three) lepton flavour states must be separately considered and the CP-violating phases of the PMNS matrix have physical significance. Historically, the possibility that the CP violation in leptogenesis may be strictly due to Dirac and/or Majorana phases of the PMNS matrix was first apparent in this regime [25–32] (for a review see, e.g., [33]).

There have been other works which have investigated the impact of low energy phases on the BAU. Indeed, CP conservation at the high-scale and CP violation at the low-scale in the context of leptogenesis can be theoretically motivated by minimal flavour violation [34, 35], flavour symmetries [36–38] or a generalised CP symmetry [39–41]. Beyond the type I

---

[1]We recall that these conditions require C-/CP violation, baryon number violation and a departure from thermal equilibrium in the production of the asymmetry [1].

seesaw mechanism, there have been other studies which connect the Dirac phase, δ, with the BAU using an extended Higgs sector [42].

The primary aims of this work are twofold:

- We revisit the possibility of producing the observed BAU where the only source of CP violation comes from the phases of the PMNS matrix and calculate the lepton asymmetry generated across seven orders of magnitude $(10^6 < T(\text{GeV}) < 10^{13})$ using our modern numerical machinery which properly incorporates radiative corrections to the light neutrino masses.

- We clarify a misunderstanding regarding the high-scale regime: as discussed above, it was initially thought that at very high scales, $T \sim 10^{12}\,\text{GeV}$, the low-energy CP phases could not produce the observed BAU. This came from the observation that in the one-flavoured regime, and barring any relation between the high-scale and low-energy CP-violating phases, the CP asymmetry is vanishing $\left(\epsilon^{(1)} = 0\right)$ for CP violation solely coming from low energy phases. This led to the conclusion that in this case no lepton asymmetry could be generated. However, the individual flavour contributions to the CP asymmetries are not zero and, even in this scenario, where flavour effects are very weak, the washouts of lepton asymmetries are flavour dependent. We show that these flavour effects may be sufficient to produce the observed baryon asymmetry. We discuss this analytically and demonstrate the viability of leptogenesis in this scenario numerically. We demonstrate with Dirac-phase leptogenesis fine-tuned cancellations in the radiative expansion of the light neutrino masses are required, however with Majorana-phase leptogenesis this is not the case. This implies the CP violation present in the low energy phases can, in principle, generate the observed matter antimatter asymmetry between $10^6 \lesssim T(\text{GeV}) \lesssim 10^{13}$.

The remainder of this work is structured as follows: in section 2 we present the relevant theoretical framework beginning with section 2.1 where we briefly review neutrino masses, mixing and radiative corrections to the light neutrino mass matrix in the type I seesaw. In section 2.2 we present the C and CP properties of the light and heavy Majorana neutrinos of the type I seesaw. This will be crucial in understanding the textures of the neutrino Yukawa matrices which contain CP-violating low energy phases and CP-conserving high energy phases. Subsequently, in section 2.3 we discuss the allowed structures of the Yukawa matrix when there is a high-scale CP symmetry. The kinetic equations and effects of flavour are discussed in section 2.4. In section 3 we revisit the link between leptonic CP violation at low energies and successful leptogenesis in the two-flavour regime (or more precisely when $10^9 \leq T\,(\text{GeV}) \leq 10^{12}$). We bring a more sophisticated set of numerical tools to more convincingly answer the question than in earlier work on the subject [25]. In section 4 we demonstrate that successful leptogenesis with only low energy CP violation is possible at much lower scales than previously considered $(T \sim 10^6\,\text{GeV})$, if one allows for fine-tuning in the light neutrino masses. In section 5 we establish that even if leptogenesis occurs at very high scales $(T \gg 10^{12}\,\text{GeV})$, then it is still possible for successful leptogenesis to result from purely low energy CP violation. We find that no fine-tuning is necessary if Majorana

θ_{13}	θ_{12}	θ_{23}	δ	Δm_{21}^2	Δm_{31}^2	Δm_{32}^2
($°$)	($°$)	($°$)	($°$)	(10^{-5}eV^2)	(10^{-3}eV^2)	(10^{-3}eV^2)
$8.52^{+0.15}_{-0.15}$	$33.63^{+0.78}_{-0.75}$	$48.7^{+1.4}_{-6.9}$	228^{+51}_{-33}	$7.40^{+0.21}_{-0.20}$	$2.515^{+0.035}_{-0.035}$	$-2.483^{+0.034}_{-0.035}$

Table 1. Best fit and 1σ ranges from a global fit to neutrino data [44].

phases play a role in the CP violation. However, purely Dirac-phase CP violation is sufficient only in scenarios with a certain degree of fine-tuning. This latter case is in stark contrast with the conclusions of the current literature.

2 Framework

2.1 Neutrino masses and mixing

Neutrino oscillation experiments have provided compelling evidence that neutrinos have small but non-zero masses and mix (for a review see, e.g., [14]). The mass and flavour states of neutrinos are misaligned, with this misalignment described by the PMNS matrix U:

$$\nu_{\alpha L} = \sum_{i=1}^{3} U_{\alpha i} \nu_{iL}, \tag{2.1}$$

where $\alpha \in \{e, \mu, \tau\}$ is the flavour of the given neutrino flavour field, $\nu_{\alpha L}$, and ν_{iL} is the left-handed component of the ith massive neutrino. Throughout this work we employ the conventional PDG parametrisation [14]:

$$U = \begin{pmatrix} c_{12}c_{13} & s_{12}c_{13} & s_{13}e^{-i\delta} \\ -s_{12}c_{23} - c_{12}s_{23}s_{13}e^{i\delta} & c_{12}c_{23} - s_{12}s_{23}s_{13}e^{i\delta} & s_{23}c_{13} \\ s_{12}s_{23} - c_{12}c_{23}s_{13}e^{i\delta} & -c_{12}s_{23} - s_{12}c_{23}s_{13}e^{i\delta} & c_{23}c_{13} \end{pmatrix} \begin{pmatrix} 1 & 0 & 0 \\ 0 & e^{i\frac{\alpha_{21}}{2}} & 0 \\ 0 & 0 & e^{i\frac{\alpha_{31}}{2}} \end{pmatrix}, \tag{2.2}$$

where $c_{ij} \equiv \cos\theta_{ij}$, $s_{ij} \equiv \sin\theta_{ij}$, δ is the Dirac phase and α_{21}, α_{31} are the Majorana phases [43] with best-fit values of θ_{12}, θ_{23}, θ_{13} and δ given in table 1. Neutrino oscillation experiments also allow to measure with precision the two independent neutrino mass squared differences Δm_{12}^2 and Δm_{31}^2 (Δm_{32}^2) which are given in table 1. In order to accommodate them, the three neutrino masses m_1, m_2 m_3 can be arranged into two possible orderings, normal ordering (NO) for $m_1 < m_2 < m_3$ and inverted ordering (IO) $m_3 < m_1 < m_2$. The ordering is not yet known although data show some mild preference for normal ordering [44].

A simple means of explaining the smallness of neutrino masses is the type I seesaw framework [5–8] in which heavy Majorana neutrinos are added to the SM particle spectrum. We shall work within a realisation of this framework which incorporates three heavy Majorana neutrinos, N_i ($i \in \{1, 2, 3\}$), such that after electroweak symmetry breaking, when the Higgs has developed a vacuum expectation value (vev) $v \approx 174$ GeV, the neutrino mass terms of the Lagrangian are given by

$$\mathcal{L}_m = -\frac{1}{2} \left(\bar{\nu}_L, \bar{N}_L^c \right) \begin{pmatrix} 0 & vY \\ vY^T & M \end{pmatrix} \begin{pmatrix} \nu_R^c \\ N_R \end{pmatrix} + \text{h.c.}, \tag{2.3}$$

where $\nu_L^T \equiv (\nu_{eL}^T, \nu_{\mu L}^T, \nu_{\tau L}^T)$ $(N_R^T \equiv (N_{1R}^T, N_{2R}^T, N_{3R}^T))$ are the light flavour (heavy mass eigenstates) neutrino fields and Y is the neutrino Yukawa matrix which couples the heavy Majorana neutrinos $N_{1,2,3}$ to the leptonic and Higgs doublets. In eq. (2.3) $(\nu_R^c)^T = ((\nu_{eR}^c)^T, (\nu_{\mu R}^c)^T, (\nu_{\tau R}^c)^T))$, $(N_L^c)^T = ((N_{1L}^c)^T, (N_{2L}^c)^T, (N_{3L}^c)^T)$, with $\nu_{lR}^c = C(\bar{\nu}_{lL})^T$, $l \in \{e, \mu, \tau\}$, and $N_{jL}^c = C(\bar{N}_{jR})^T$ for $j \in \{1, 2, 3\}$. Finally, C denotes charge conjugation matrix.

The mass terms in eq. (2.3) are written in the basis where the charged lepton Yukawa couplings are flavour diagonal, which we use throughout the present study. We shall also work, without loss of generality, in a basis in which M is diagonal and positive.

To first order in the seesaw expansion, the tree-level light neutrino mass matrix is given by

$$m_\nu^{\text{tree}} = v^2 Y M^{-1} Y^T, \tag{2.4}$$

where we employ the sign conventions of [25]. In the generic type I seesaw, there is no symmetry protecting the tree-level neutrino masses from radiative corrections. Moreover, the one-loop radiative corrections may be comparable to the tree-level mass. For this reason, when exploring the parameter space of type I seesaw models, it is relevant to compute the additional contribution to the light masses arising from the one-loop self-energy[2] [45–47] (see also, e.g., [48]):

$$m_\nu^{\text{1-loop}} = -Y \frac{M}{32\pi^2} \left(\frac{\log\left(\frac{M^2}{m_H^2}\right)}{\frac{M^2}{m_H^2} - 1} + 3 \frac{\log\left(\frac{M^2}{m_Z^2}\right)}{\frac{M^2}{m_Z^2} - 1} \right) Y^T, \tag{2.5}$$

where m_Z and m_H are the Z and Higgs boson masses respectively. With these included, the light neutrino mass matrix is given by

$$\begin{aligned} m_\nu &= m_\nu^{\text{tree}} + m_\nu^{\text{1-loop}} \\ &= v^2 Y f(M) Y^T, \\ &= m_D f(M) m_D^T, \end{aligned} \tag{2.6}$$

where $m_D \equiv vY$ and

$$f(M) \equiv M^{-1} - \frac{M}{32\pi^2 v^2} \left(\frac{\log\left(\frac{M^2}{m_H^2}\right)}{\frac{M^2}{m_H^2} - 1} + 3 \frac{\log\left(\frac{M^2}{m_Z^2}\right)}{\frac{M^2}{m_Z^2} - 1} \right). \tag{2.7}$$

From the structure of eq. (2.5), we observe that the tree and one-loop level contributions to the light neutrino masses are both quadratic in the Yukawa couplings. The only suppression of the one-loop derives from the $\mathcal{O}(10^{-2})$ loop-factor. Furthermore, from eq. (2.7) it follows that the one-loop contribution generically tends to reduce the tree-level mass. This suggests that there exists the possibility of a cancellation between the tree and

---

[2]In this expression terms of order $m_\nu^{\text{tree}} \frac{Y^2}{32\pi^2}$ have been neglected. This is equivalent to neglecting the tree-level mass when computing the one-loop contribution. Thus, the physically irrelevant divergent pieces and renormalisation-scale dependent pieces are not present in the expression we give.

one-loop contributions. In this work we do not preclude the possibility that these cancellations may be present. The higher-order corrections to the light neutrino masses are generally suppressed by additional loop factors and couplings and generally do not experience fine-tuned cancellations, instead they contribute in the usual way to the perturbative expansion. We define a fine-tuning measure, $\mathcal{F}$, to quantify the level of cancellation:

$$\mathcal{F} \equiv \frac{m_\nu^{\text{1-loop}}}{m_\nu^{\text{tree}} + m_\nu^{\text{1-loop}}}. \tag{2.8}$$

The one-loop correct light neutrino mass matrix of eq. (2.6), m_ν, may be transformed into a positive diagonal form (denoted by a caret) using the Takagi factorisation

$$\hat{m}_\nu = U^\dagger m_\nu U^*, \tag{2.9}$$

such that $\hat{m}_\nu = \text{diag}(m_1, m_2, m_3)$, with m_i the mass corresponding to ν_i. By analogy with the method of Casas and Ibarra [49], we parametrise the Yukawa matrix to include the relevant radiative corrections as [50]

$$Y = \frac{1}{v} U \sqrt{\hat{m}_\nu} R^T \sqrt{f(M)^{-1}}, \tag{2.10}$$

where R is a 3×3 complex orthogonal matrix. Explicitly, we choose to work with the parametrisation:[3]

$$R = \begin{pmatrix} 1 & 0 & 0 \\ 0 & c_1 & s_1 \\ 0 & -s_1 & c_1 \end{pmatrix} \begin{pmatrix} c_2 & 0 & s_2 \\ 0 & 1 & 0 \\ -s_2 & 0 & c_2 \end{pmatrix} \begin{pmatrix} c_3 & s_3 & 0 \\ -s_3 & c_3 & 0 \\ 0 & 0 & 1 \end{pmatrix}, \tag{2.11}$$

where $c_i = \cos w_i$, $s_i = \sin w_i$ and the complex angles are given by $w_i = x_i + iy_i$ ($i \in \{1, 2, 3\}$).

2.2 C and CP properties of Majorana neutrinos

As we focus on the possibility that low-scale CP phases are responsible for the BAU, the C and CP properties of neutrinos will be crucial in understanding the structure of the R-matrix which results in the CP conservation of the high-scale phases. In the type I seesaw, the light (ν_i) and the heavy (N_i) neutrino mass states are both Majorana in nature and thus satisfy the following conditions:

$$\begin{aligned} C\overline{\nu}_i^T &= \nu_i, \\ C\overline{N}_i^T &= N_i, \end{aligned} \tag{2.12}$$

where C denotes the charge conjugation matrix.

Following [26], we express the CP-conjugated neutrino fields in terms of the CP operator U_{CP} as

$$\begin{aligned} U_{\text{CP}} N_i\left(x\right) U_{\text{CP}}^\dagger &= i\rho_i^N N_i\left(x'\right), \\ U_{\text{CP}} \nu_i\left(x\right) U_{\text{CP}}^\dagger &= i\rho_i^\nu \nu_i\left(x'\right), \end{aligned} \tag{2.13}$$

---

[3]A phase factor $\xi = \pm 1$ could have been included in the definition of R to allow for both the cases $\det(R) = \pm 1$ however we have chosen to extend the range of the Majorana phases such that the choice of signs of $\det(R)$ have effectively already been incorporated.

where x' is the parity-transformed coordinate and $i\rho_i^N = \pm i$ and $i\rho_i^\nu = \pm i$ are the CP parities of the respective Majorana fields. The conditions for CP invariance impose the following restrictions on the elements of the matrix of neutrino Yukawa couplings (setting the unphysical phases in the CP transformations of the lepton and Higgs doublets to unity) is given by,

$$Y_{\alpha i}^* = Y_{\alpha i}\rho_i^N, \tag{2.14}$$

and on the elements of the PMNS matrix [51]:

$$U_{\alpha j}^* = U_{\alpha j}\rho_j^\nu, \ j \in \{1,2,3\}, \ \alpha \in \{e,\mu,\tau\}. \tag{2.15}$$

From the parametrisation of the Yukawa matrix of eq. (2.10), this imposes the following conditions on the elements of the R-matrix [26]:

$$R_{ij}^* = R_{ij}\rho_i^N\rho_j^\nu, \ i,j \in \{1,2,3\}. \tag{2.16}$$

The leptogenesis scenarios considered in this work have CP violation provided only by the phases of the PMNS matrix. This corresponds to imposing the condition of eq. (2.16) onto the R-matrix but not the condition eq. (2.15) on U. In these scenarios the values of the Dirac and Majorana phases of the PMNS matrix determine the success of leptogenesis. One should bear in mind, however, that there are certain intuitively unexpected possibilities for CP violation in (non-resonant) leptogenesis even when the PMNS- and R-matrices are CP-conserving, i.e., conditions (eq. (2.15)) and (eq. (2.16)) are individually fulfilled and the elements U_{lj} and R_{jk} are real or purely imaginary [26].[4]

CP violation due to the Dirac phase δ can only be practically investigated in neutrino oscillation experiments. There has been a slight statistical preference from the existing data for maximally CP-violating $\delta \sim 270°$. This hint has been obtained from the combination of results from long-baseline experiments such as T2K [52] and NOνA [53] with reactor experiments like Daya-Bay [54], RENO [55] and Double-Chooz [56]. In principle, the difference in oscillation probabilities [57–59],

$$A_{\mathrm{CP}}^{\alpha,\beta} \equiv P(\nu_\alpha \to \nu_\beta) - P(\overline{\nu}_\alpha \to \overline{\nu}_\beta) \quad (\alpha \neq \beta), \tag{2.17}$$

is a measure of CP violation in neutrino oscillations in vacuum and can be measured experimentally. For vacuum oscillations in the three-neutrino case we have [60]

$$A_{\mathrm{CP}}^{e,\mu} = 4J_{\mathrm{CP}}F_{\mathrm{osc}}^{\mathrm{vac}}, \tag{2.18}$$

$$F_{\mathrm{osc}}^{\mathrm{vac}} \equiv \sin\left(\frac{\Delta m_{21}^2}{2E}L\right) + \sin\left(\frac{\Delta m_{32}^2}{2E}L\right) + \sin\left(\frac{\Delta m_{13}^2}{2E}L\right), \tag{2.19}$$

$$J_{\mathrm{CP}} \equiv \Im\left[U_{e1}U_{\mu 2}U_{e2}^*U_{\mu 1}^*\right]. \tag{2.20}$$

---

[4]This unusual possibility is realised when ρ_i^N and ρ_j^ν are fixed by conditions (eq. (2.14)) and (eq. (2.15)), but the product of the so fixed values of ρ_i^N and ρ_j^ν differs from the value of $\rho_i^N\rho_j^\nu$ in (eq. (2.16)) [26]. Under these conditions the low energy PMNS matrix U and the high-scale R-matrix are individually CP-conserving, but the interplay between the two in leptogenesis is CP-violating.

$J_{\rm CP}$ is the analogue of the Jarlskog invariant for the lepton sector, which gives a parametrisation-independent measure of CP violation in neutrino oscillations, L is the distance travelled by the neutrinos, E the neutrino energy and $\Delta m_{ij}^2 \equiv m_i^2 - m_j^2$. In the case of CP-invariance we have $\delta = 0, \pi$ and therefore $J_{\rm CP} = 0$. By measuring, for example, $A_{\rm CP}^{e,\mu}$, one can determine $J_{\rm CP}$ which has the following expression in the standard parametrisation of the PMNS matrix:

$$J_{\rm CP} = \frac{1}{4} \sin 2\theta_{12} \sin 2\theta_{23} \cos^2 \theta_{13} \sin \theta_{13} \sin \delta. \tag{2.21}$$

The best-fit value and 1σ uncertainty of $J_{\rm CP}$ reported in [44] are

$$J_{\rm CP}^{\rm max} = 0.0329 \pm 0.0007 \, (\pm 1\sigma). \tag{2.22}$$

In the longer term, the next generation of neutrino oscillation experiments such as DUNE [61] and T2HK [62], will be able to measure the Dirac CP-violating phase δ with greater precision and determine whether CP-symmetry is indeed violated in the lepton sector.

Information on CP-violating Majorana phases can, in principle, be obtained in neutrinoless double beta decay experiments [63–65] (see, however, also [66]). These experiments are the most sensitive probes of the possible Majorana nature of massive neutrinos. They can also provide information on the neutrino mass ordering [67] (see also [65]). The rate of neutrinoless double beta decay is given by (see, e.g., [68])

$$\frac{\Gamma_{0\nu\beta\beta}}{\log 2} = \frac{G_{01}}{m_e^2} |\mathcal{A}|^2, \tag{2.23}$$

where G_{01} is a kinematic factor and $\mathcal{A}$ denotes the amplitude which has the following form

$$\mathcal{A} \propto \sum_{i=1}^{3} m_i U_{ei}^2 \mathcal{M}^{0\nu\beta\beta}(m_i) + \sum_{i=1}^{3} M_i V_{ei}^2 \mathcal{M}^{0\nu\beta\beta}(M_i). \tag{2.24}$$

The amplitude is dependent on the nuclear matrix elements $\mathcal{M}^{0\nu\beta\beta}$ for which $\mathcal{M}^{0\nu\beta\beta}(m_i) \approx \mathcal{M}^{0\nu\beta\beta}(0) \gg \mathcal{M}^{0\nu\beta\beta}(M_i)$ if $M_i \gg 10^3$ MeV (see, e.g., [68, 69]), which shall always be the case in this work. The mixing elements V_{ei} for the heavy states are $\mathcal{O}(m_D/M)$ and thus the second term of eq. (2.24) is $\mathcal{O}(m_D^2/M)\mathcal{M}^{0\nu\beta\beta}(M_i) \sim \mathcal{O}(m_i)\mathcal{M}^{0\nu\beta\beta}(M_i)$. As $U_{ei} \sim \mathcal{O}(1)$, the second term is negligible in comparison with the first and we find [70] (see e.g., [51]):

$$A \propto \langle m_\nu \rangle \equiv m_1 U_{e1}^2 + m_2 |U_{e2}|^2 e^{i\alpha_{21}} + m_3 |U_{e3}|^2 e^{i(\alpha_{31} - 2\delta)}, \tag{2.25}$$

where $\langle m_\nu \rangle$ is the neutrinoless double beta decay effective Majorana mass in the case of 3-neutrino mixing. In the case of CP-invariance we have $\alpha_{21} = k\pi$, $\alpha_{31} = q\pi$, $k, q = 0, 1, 2, \ldots$ [71–73].[5] The most stringent upper bound on $|\langle m_\nu \rangle|$ was reported by the KamLAND-Zen collaboration [74] searching for neutrinoless double beta decay of ^{136}Xe:

$$|\langle m_\nu \rangle| < (0.061 - 0.165) \text{ eV}, \tag{2.26}$$

---

[5]Thus, in order for a value of $\alpha_{21(31)}$ to be CP-violating both $\sin \frac{\alpha_{21(31)}}{2}$ and $\cos \frac{\alpha_{21(31)}}{2}$ at this value should be different from zero.

where the uncertainty in the knowledge of the nuclear matrix element of ^{136}Xe decay have been accounted for. In terms of the half-lives for neutrinoless double beta decay the best lower limits are: for germanium-76, tellurium-130, and xenon-136: $T_{1/2}^{0\nu} > 8.0 \times 10^{25}$ yr (reported by the GERDA-II collaboration), $T_{1/2}^{0\nu} > 1.5 \times 10^{25}$ yr (from the combined results of the Cuoricino, CUORE-0, and CUORE experiments), and $T_{1/2}^{0\nu} > 1.07 \times 10^{26}$ yr (from the KamLAND-Zen collaboration), with all limits given at the 90% CL. Most importantly, a large number of experiments of a new generation aim at sensitivities to $|\langle m_\nu \rangle| \sim (0.01 \div 0.05)$ eV (see, e.g., [69, 75]): CUORE (^{130}Te), SNO+ (^{130}Te), GERDA (^{76}Ge), MAJORANA (^{76}Ge), LEGEND (^{76}Ge), SuperNEMO (^{82}Se, ^{150}Nd), KamLAND-Zen (^{136}Xe), EXO and nEXO (^{136}Xe), PANDAX-III (^{136}Xe), NEXT (^{136}Xe), AMoRE (^{100}Mo), MOON (^{100}Mo), CANDLES (^{48}Ca), XMASS (^{136}Xe), DCBA (^{82}Se, ^{150}Nd), ZI-COS (^{96}Zr), etc. The GERDA-II and KamLAND-Zen experiments have already provided the best lower limits on the double beta decay half-lives of ^{76}Ge and ^{136}Xe. The experiments listed above aim to probe the ranges of predictions of $|\langle m_\nu \rangle|$ corresponding to neutrino mass spectra of quasi-degenerate type and with inverted ordering (see, e.g., [14]).

The primary focus of this work is to answer the question: *at what scales can low-energy CP-violating phases produce the observed BAU?* We shall show that the scale of successful leptogenesis in the case of interest may indeed vary across many orders of magnitude from $10^6 - 10^{13}$ GeV. The observation of low-scale leptonic Dirac CP violation, in combination with the positive determination of the Majorana nature of the massive neutrinos, would make more plausible, but will not be a proof of, the existence of high-scale thermal leptogenesis. These remarkable discoveries would indicate, in particular, that thermal leptogenesis *could* produce the BAU with the requisite CP violation provided by the Dirac CP-violating phase in the neutrino mixing matrix.

2.3 CP-conserving R-matrix and the structure of the light neutrino mass matrix

If the orthogonal matrix R is allowed to have large elements, then the scale of leptogenesis may be lowered to $M_1 \sim 10^6$ GeV [76–78]. In such scenarios, care must be taken with the radiative corrections to the light neutrino masses which may grow large (and non-negligible) with the elements of the R-matrix. One can either impose a near-lepton-number-symmetry to prevent this (see [77]), or more generically, incorporate the one-loop contribution to the light neutrino masses (in the manner we have discussed) and remain agnostic about fine-tuned cancellations between the tree-level and one-loop contributions. We proceed with this approach following the attitude taken in [78], in which the figure $M_1 \sim 10^6$ GeV was first demonstrated.

$$R \approx \begin{pmatrix} R_{11} & R_{12} & R_{13} \\ \pm i R_{22} & R_{22} & R_{23} \\ -R_{22} & \pm i R_{22} & \pm i R_{23} \end{pmatrix}, \tag{2.27}$$

$|R_{22}| \gg |R_{1i}|, |R_{23}|$ for $i \in \{1, 2, 3\}$. The cancellation of large tree-level and large one-loop light neutrino mass matrices occurs as a result of relations between the magnitudes and phases of the R-matrix elements which lead to the following structure for the Dirac mass

matrix:

$$m_D \sqrt{f} = \left(\Delta, \, u, \, \pm iu \right), \tag{2.28}$$

with $\Delta = U \left(\sqrt{m_1} R_{11}, \sqrt{m_2} R_{12}, \sqrt{m_3} R_{13} \right)^T$ and $u = U \left(\pm i \sqrt{m_1} R_{22}, \sqrt{m_2} R_{22}, \sqrt{m_3} R_{23} \right)^T$, such that $|\Delta_i| \ll |u_j|$, $i, j \in \{1, 2, 3\}$. We may rewrite the tree and one-loop masses in terms of this relatively simple matrix $m_D \sqrt{f}$, such that

$$m^{\text{tree}} = \left(m_D \sqrt{f} \right) M^{-1} f^{-1} \left(m_D \sqrt{f} \right)^T, \tag{2.29}$$

where the commutativity of the diagonal matrices M and f has been exploited and

$$m^{\text{1-loop}} = \left(m_D \sqrt{f} \right) \left(f - M^{-1} \right) f^{-1} \left(m_D \sqrt{f} \right)^T. \tag{2.30}$$

This ensures that the sum of the tree-level and one-loop masses is

$$\begin{aligned} m_\nu &= m_D \sqrt{f} \left(m_D \sqrt{f} \right)^T \\ &= \Delta \Delta^T. \end{aligned} \tag{2.31}$$

Due to the relative smallness of the elements of Δ, the matrix m_ν may be considerably smaller than m^{tree}. Immediately, we have

$$m^{\text{tree}} = -m^{\text{1-loop}} + \mathcal{O}(\Delta^2), \tag{2.32}$$

which is an explicit expression of the fine-tuned cancellation.

As the R-matrix structure of eq. (2.27) is required for successful leptogenesis at intermediate scales, we are tasked with the problem of finding the R-matrices which assume this form and obey the CP-invariance conditions of eq. (2.16). We intend to translate the conditions in eq. (2.27) and eq. (2.16) into constraints on x_i and y_i. However, we know *a priori* from the work of [78] that one must have $y_2 \sim 0°$ and $y_1 \gtrsim 180°$, $y_3 \gtrsim 180°$ to produce the relative magnitudes of the elements of R in eq. (2.27), crucial to the successful production of the observed baryon asymmetry.

We begin with the elements

$$R_{22} = \cos w_1 \cos w_3 - \sin w_1 \sin w_2 \sin w_3, \tag{2.33}$$

and

$$R_{31} = -\cos w_1 \cos w_3 \sin w_2 + \sin w_1 \sin w_3, \tag{2.34}$$

which result from the expansion of the R-matrix parametrised as in eq. (2.11). The condition of eq. (2.27) that $R_{22} \approx -R_{31}$ implies that $\sin w_2 \approx 1$, which in turn imposes $\sin x_2 \approx 1$ and $y_2 \approx 0°$. In order to simplify future expressions, we promote the condition on y_2 to the exact equality $y_2 = 0°$. With conditions on x_2 and y_2 determined, we now examine

$$R_{13} = \cos x_2 \left(\cos x_1 \cosh y_1 - i \sin x_1 \sinh y_1 \right). \tag{2.35}$$

According to the condition eq. (2.16), R_{13} (like all the elements of R) must be purely real or imaginary and thus we should choose one of, $\cos x_1 = 0$ or $\sin x_1 = 0$. We exclude the possibility of $y_1 = 0$ for the reason given above. Likewise, consider

$$R_{11} = \cos x_2 \left(\cos x_3 \cosh y_3 - i \sin x_3 \sinh y_3\right), \tag{2.36}$$

and select $\cos x_3 = 0$ or $\sin x_3 = 0$ by the same reasoning.

In summary, we have the following set of constraints

$$
\begin{aligned}
\cos x_2 &\approx 0 \quad \text{and } y_2 = 0, \\
|\cos x_1| &= 0 \text{ or } 1, \\
|\cos x_3| &= 0 \text{ or } 1,
\end{aligned}
\tag{2.37}
$$

which lead to an R-matrix of purely real and imaginary components and are therefore good candidates for CP-invariant R-matrices. We shall make use of these conditions in considerations where enhancement of the R-matrix is necessary for successful leptogenesis.

2.4 The effects of flavour and scale in leptogenesis

In addition to explaining the smallness of neutrino masses, the type I seesaw provides a framework under which the matter-antimatter asymmetry of the Universe is explicable. The heavy Majorana neutrinos N_i may undergo out-of-equilibrium, C-/CP- and lepton-number-violating decays in the early Universe. The resulting leptonic matter-antimatter asymmetry is then partially converted into a baryonic asymmetry by SM sphaleron processes which violate $B + L$ but conserve $B - L$. The baryon asymmetry, which quantifies the excess of matter over antimatter in the Universe, is defined by

$$\eta_B \equiv \frac{n_B - n_{\overline{B}}}{n_\gamma}, \tag{2.38}$$

where n_B, $n_{\overline{B}}$ and n_γ are the number densities of baryons, antibaryons and photons respectively. This quantity has been measured using two independent methods. There is the measurement of the baryon-to-photon ratio from Big-Bang nucleosynthesis (BBN), a process which occurs when the temperature of the Universe drops below $T \lesssim 1$ MeV [79]:

$$\eta_{B\,\text{BBN}} = (5.80 - 6.60) \times 10^{-10}.$$

In complement, there is the determination of η_B from Cosmic Microwave Background radiation (CMB) data [80] for which the relevant cosmological period is that of recombination, for which $T \lesssim 1$ eV:

$$\eta_{B\,\text{CMB}} = (6.02 - 6.18) \times 10^{-10}.$$

Throughout our numerical study we apply the latter, more precisely measured value.

In the simplest scenario, thermal leptogenesis describes the time evolution of a lepton asymmetry as a result of the CP-violating decays of the heavy Majorana neutrinos. In these processes, the lepton and anti-lepton states are

$$|i\rangle \equiv \sum_\alpha C_{i\alpha} |\alpha\rangle, \quad |\bar{i}\rangle \equiv \sum_\alpha \overline{C}_{i\alpha} |\overline{\alpha}\rangle, \tag{2.39}$$

where, at tree-level, the projection coefficients are expressed as

$$C_{i\alpha} = \overline{C}_{i\alpha} = \frac{Y_{\alpha i}}{\sqrt{(Y^\dagger Y)_{ii}}}, \tag{2.40}$$

for $i \in \{1, 2, 3\}$ and $\alpha \in \{e, \mu, \tau\}$. The simplest scenario for leptogenesis is the *single flavour* regime, in which, the leptons resulting from the decay of each heavy Majorana neutrino N_i are always found in the coherent superposition of flavours described by the corresponding $|i\rangle$. This condition is valid if flavour-dependent interactions mediated by the SM charged lepton Yukawa couplings are negligible. This is usually a sufficiently good approximation for temperatures $T \gg 10^{12}$ GeV, when the charged lepton Yukawa interactions proceed at a slower rate than the expansion of the Universe. However, in this work, we shall demonstrate that such an approximation fails in certain regions of the model parameter space.

The single flavoured Boltzmann equations for thermal leptogenesis provide a semi-classical description of the time evolution of the heavy neutrino densities, n_{N_i} ($i \in \{1, 2, 3\}$), and the lepton asymmetry, n_{B-L}.[6] Introducing the parameter $z \equiv M_1/T$, which increases monotonically with time, these kinetic equations are written

$$\begin{aligned}
\frac{dn_{N_i}}{dz} &= - D_i(n_{N_i} - n_{N_i}^{\text{eq}}), \\
\frac{dn_{B-L}}{dz} &= \sum_{i=1}^{3} \left(\epsilon^{(i)} D_i(n_{N_i} - n_{N_i}^{\text{eq}}) - W_i n_{B-L} \right).
\end{aligned} \tag{2.41}$$

In general, the decay parameter D_i, describing the decay of N_i is defined in terms of the heavy neutrino decay rate $\Gamma_i \equiv \Gamma_i \left(N_i \to \phi^\dagger l_i \right)$ (with ϕ and l_i the Higgs and lepton doublets), the CP-conjugate rate, $\overline{\Gamma}_i$, and Hubble rate, H [11]:

$$D_i \equiv \frac{\Gamma_i + \overline{\Gamma}_i}{Hz}. \tag{2.42}$$

Likewise, the washout factor is defined in terms of the heavy neutrino inverse decay rate Γ_i^{ID} and the CP-conjugate inverse decay rates $\overline{\Gamma}_i^{\text{ID}}$

$$W_i \equiv \frac{1}{2} \frac{\Gamma_i^{\text{ID}} + \overline{\Gamma}_i^{\text{ID}}}{Hz}. \tag{2.43}$$

Finally, the CP-asymmetry parameter $\epsilon^{(i)}$ is defined as[7]

$$\epsilon^{(i)} \equiv -\frac{\Gamma_i - \overline{\Gamma}_i}{\Gamma_i + \overline{\Gamma}_i} = -\frac{3}{16\pi (Y^\dagger Y)_{ii}} \sum_{j \neq i} \Im \left[\left(Y^\dagger Y \right)_{ij}^2 \right] \frac{\xi(x_j/x_i)}{\sqrt{x_j/x_i}}, \tag{2.44}$$

with

$$x_i \equiv M_i^2/M_1^2, \quad \xi(x) \equiv \frac{2}{3} x \left[(1+x) \log \left(\frac{1+x}{x} \right) - \frac{2-x}{1-x} \right]. \tag{2.45}$$

---

[6]All number densities are normalised to a volume containing a single heavy Majorana neutrino in ultra-relativistic thermal equilibrium.

[7]Note that the Yukawas enter only in the combination $Y^\dagger Y$ and hence, from the eq. (2.10), there is no dependence on the PMNS matrix, U. Thus, in the one-flavour case, there can be no contribution to the CP-asymmetry from the Dirac and Majorana phases.
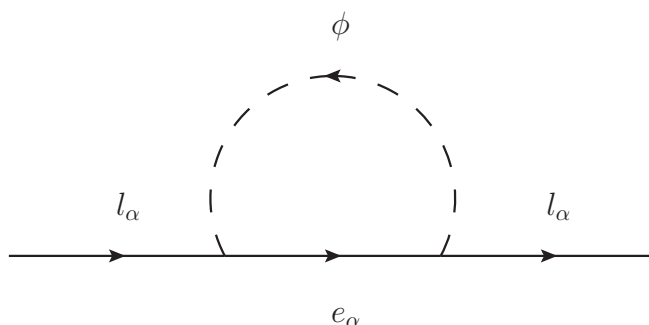
Figure 1. The one-loop contribution to the thermal-width for left-handed leptonic doublet of flavour α (l_α) through the right-handed singlet of the same flavour (e_α).

As discussed, the light neutrino masses may have an accidental cancellation in the tree-level mass that makes it comparable to the one-loop mass. However, there is no reason to expect an accidental cancellation like this to occur in the CP-asymmetry. This is because the cancellation in the light neutrino masses was due to the presence of terms of the form $YM^{-1}Y^T$ while in the CP-asymmetries, the Yukawa matrix is multiplied by their conjugates in combinations of $Y^\dagger Y$ and therefore a similar cancellation cannot occur. As such, the higher-order corrections to the CP-asymmetry should not be any more significant in our case than they usually are.

Eq. (2.41) describes the time evolution of lepton number density asymmetry, n_{B-L}, from an initial value (usually it is assumed that there is a vanishing initial abundance) to a final value, $n_{B-L}(z_{\text{final}})$. The final leptonic asymmetry is then partially converted into a baryonic asymmetry through sphaleron processes. This is expressed quantitatively by the relation $\eta_B \approx a/f \times n_{B-L} \approx 10^{-2} n_{B-L}$ [11], where $a = 28/79$ describes the partial conversion of the $B - L$ asymmetry into a baryon asymmetry by sphaleron processes, and $f \equiv n_\gamma^{\text{rec}}/n_\gamma^* = 2387/86$ accounts for the dilution of the asymmetry due the change of photon densities (n_γ) between leptogenesis ($n_\gamma = n_\gamma^*$) and recombination ($n_\gamma = n_\gamma^{\text{rec}}$).

If the era of leptogenesis is lowered below $T \sim 10^{12}\,\text{GeV}$, the interactions of the tau charged lepton, mediated by its SM Yukawa coupling, come into thermal equilibrium. The effect is that the τ-component of each $|i\rangle$ experiences relatively rapid interactions with the early Universe plasma. The left-handed τ component is rapidly converted to a right-handed τ via scattering with the Higgs. Similarly, the reverse process repopulates the τ asymmetry density at the same rate. This rate is determined by the imaginary part of the thermal self-energy of τ, $\Im(\Lambda_\tau)$, which by the optical theorem determines the mean free path of the τ state (see figure 1). When this process is sufficiently rapid, the coherent superposition of flavours is destroyed and the τ component can no longer contribute at the level of amplitudes to the decay and inverse decay processes with e and μ (which form a single coherent flavour state which we shall refer to as $\tau^\perp$ such that $\langle \tau | \tau^\perp \rangle = 0$). Instead τ undergoes decay and inverse decay as a separate decoherent state. Correspondingly, the kinetic equations must separately describe the time evolution of $n_{\tau\tau}$ and $n_{\tau^\perp\tau^\perp}$ and the total baryon asymmetry is simply the sum: $n_{B-L} = n_{\tau\tau} + n_{\tau^\perp\tau^\perp}$. This is the *two-flavoured*

regime and the Boltzmann equations are given by

$$\frac{dn_{N_i}}{dz} = -D_i(n_{N_i} - n_{N_i}^{\text{eq}}),$$

$$\frac{dn_{\tau\tau}}{dz} = \sum_i \left(\epsilon_{\tau\tau}^{(i)} D_i(n_{N_i} - n_{N_i}^{\text{eq}}) - p_{i\tau} W_i n_{\tau\tau} \right),$$

$$\frac{dn_{\tau^\perp\tau^\perp}}{dz} = \sum_i \left(\epsilon_{\tau^\perp\tau^\perp}^{(i)} D_i(n_{N_i} - n_{N_i}^{\text{eq}}) - p_{i\tau^\perp} W_i n_{\tau^\perp\tau^\perp} \right),$$

(2.46)

where $p_{i\alpha} \equiv |C_{i\alpha}|^2$, $\overline{p}_{i\alpha} \equiv |\overline{C}_{i\alpha}|^2$ are the projection probabilities expected from the decoherence - the classical measurement of τ by the early Universe plasma. Furthermore, the CP-asymmetries are

$$\epsilon_{\alpha\alpha}^{(i)} = -\frac{p_{i\alpha}\Gamma_i - \overline{p}_{i\alpha}\overline{\Gamma}_i}{\Gamma_i + \overline{\Gamma}_i},$$

(2.47)

for $\alpha = \tau^\perp, \tau$. Analogously, there exists the possibility that the out-of-equilibrium decays of the heavy Majorana neutrinos occur at temperatures where the SM muon Yukawa interactions has thermalised $T \sim 10^9$ GeV and the *three-flavoured* Boltzmann equations are the relevant kinetic equations. This possibility was explored in [76] and it was shown that thermal leptogenesis can be lowered to $T \sim 10^8$ GeV.

It has been shown [22, 23, 81, 82, 86] that the density matrix equations produce a more physically accurate description of leptogenesis where the density matrix may be expressed as

$$n \equiv \sum_{\alpha,\beta} n_{\alpha\beta} |\alpha\rangle\langle\beta|,$$

(2.48)

where $|\alpha\rangle$ are states of definite lepton flavour, defining the flavour basis. Using this description, the diagonal elements, $n_{\alpha\alpha}$, are the differences of the normalised densities of α and $\overline{\alpha}$ particles such that $n_{B-L} = \text{Tr}\, n$. The off-diagonals describe the degree of coherence between the flavour states. The advantage of a density matrix description is that decoherence effects are easily incorporated and as such, the dynamical process by which different flavour states decohere is readily incorporated into the equations. This allows for a single set of equations with solutions which transition between flavour-regimes as appropriate. Furthermore, the equations should remain accurate even in the regions of transition where the interactions leading to decoherence are not infinitely fast.

Explicitly, the *density matrix equations* of leptogenesis are [22, 23, 81, 82, 86]

$$\frac{dn_{N_i}}{dz} = -D_i(n_{N_i} - n_{N_i}^{\text{eq}})$$

$$\frac{dn_{\alpha\beta}}{dz} = \sum_i \left(\epsilon_{\alpha\beta}^{(i)} D_i(n_{N_i} - n_{N_i}^{\text{eq}}) - \frac{1}{2} W_i \left\{ P^{0(i)}, n \right\}_{\alpha\beta} \right)$$

$$- \frac{\Im(\Lambda_\tau)}{Hz} \left[\begin{pmatrix} 1 & 0 & 0 \\ 0 & 0 & 0 \\ 0 & 0 & 0 \end{pmatrix}, \left[\begin{pmatrix} 1 & 0 & 0 \\ 0 & 0 & 0 \\ 0 & 0 & 0 \end{pmatrix}, n \right] \right]_{\alpha\beta}$$

$$- \frac{\Im(\Lambda_\mu)}{Hz} \left[\begin{pmatrix} 0 & 0 & 0 \\ 0 & 1 & 0 \\ 0 & 0 & 0 \end{pmatrix}, \left[\begin{pmatrix} 0 & 0 & 0 \\ 0 & 1 & 0 \\ 0 & 0 & 0 \end{pmatrix}, n \right] \right]_{\alpha\beta},$$

(2.49)

where the projection matrices are

$$P^{0(i)}_{\alpha\beta} \equiv C_{i\alpha}C^*_{i\beta}, \tag{2.50}$$

which generalise the notion of the projection probability and appear in the double commutator structure. The double-commutator structures in eq. (2.49) give rise to an exponentially damping term proportional to $\Im(\Lambda_\alpha)/Hz$ for the equations describing the off-diagonal elements of n. In the flavour basis, if these terms are dominant, the density matrix is driven towards a diagonal form. The CP-asymmetry parameters are [21, 22, 81, 83–87]

$$\epsilon^{(i)}_{\alpha\beta} = \frac{3}{32\pi (Y^\dagger Y)_{ii}} \sum_{j\neq i} \left\{ i[Y_{\alpha i}Y^*_{\beta j}(Y^\dagger Y)_{ji} - Y^*_{\beta i}Y_{\alpha j}(Y^\dagger Y)_{ij}]f_1\left(\frac{x_j}{x_i}\right) \right.$$
$$\left. + i[Y_{\alpha i}Y^*_{\beta j}(Y^\dagger Y)_{ij} - Y^*_{\beta i}Y_{\alpha j}(Y^\dagger Y)_{ji}]f_2\left(\frac{x_j}{x_i}\right) \right\}, \tag{2.51}$$

where

$$f_1\left(\frac{x_j}{x_i}\right) \equiv \frac{\xi\left(\frac{x_j}{x_i}\right)}{\sqrt{\frac{x_j}{x_i}}}, \quad f_2\left(\frac{x_j}{x_i}\right) \equiv \frac{2}{3\left(\frac{x_j}{x_i}-1\right)}. \tag{2.52}$$

The diagonal components of the $\epsilon^{(i)}$ matrix simplify to the following form

$$\epsilon^{(i)}_{\alpha\alpha} = \frac{3}{16\pi (Y^\dagger Y)_{ii}} \sum_{j\neq i} \left\{ \Im\left[Y_{\alpha i}{}^* Y_{\alpha j}(Y^\dagger Y)_{ij}\right] f_1\left(\frac{x_j}{x_i}\right) + \Im\left[Y_{\alpha i}{}^* Y_{\alpha j}(Y^\dagger Y)_{ji}\right] f_2\left(\frac{x_j}{x_i}\right) \right\}. \tag{2.53}$$

3 Leptogenesis in the regime $10^9 < M_1(\text{GeV}) < 10^{12}$

In this section, we explore the possibility that successful leptogenesis derives solely from the CP-violating PMNS phases and the mass scale is between $10^9 \leq M_1$ (GeV) $\leq 10^{12}$, which generally corresponds to the two-flavour regime. Historically, the link between low-energy CP violation and the baryon asymmetry was first established in this regime and thus our main purpose in this section is to revisit the scenario with more robust numerical methods than have previously been applied. We shall perform a comprehensive exploration of the parameter space for a model with three heavy Majorana neutrinos in both the normal ordered and inverted ordered scenarios. We shall then investigate a subset of scenarios in which only the Dirac or only the Majorana phases are varied.

3.1 Results of parameter exploration

In this particular explorations of the parameter space, we fix M_1 and vary M_2 and M_3 such that $M_3 > 3M_2 > 9M_1$, ensuring that resonant regimes are avoided [13, 76, 87, 89–91]. We choose to set $M_1 = 10^{10}$ GeV, this being typical of the mass window under consideration.

We fix, $x_1 = 90°$ and $x_3 = 180°$ and $y_2 = 0°$ such that there is a complete leptonic CP-symmetry when $\delta = 0°$, $\alpha_{21} = 180°$ and $\alpha_{31} = 0°$.[8] With the specified parameters

---

[8]This choice of parameters for the low-energy phases is made such that the CP-symmetry holds for the Yukawa matrix when the R-matrix is taken in to account. It would not suffice to choose, eg., $\delta = \alpha_{21} = \alpha_{31} = 0°$.
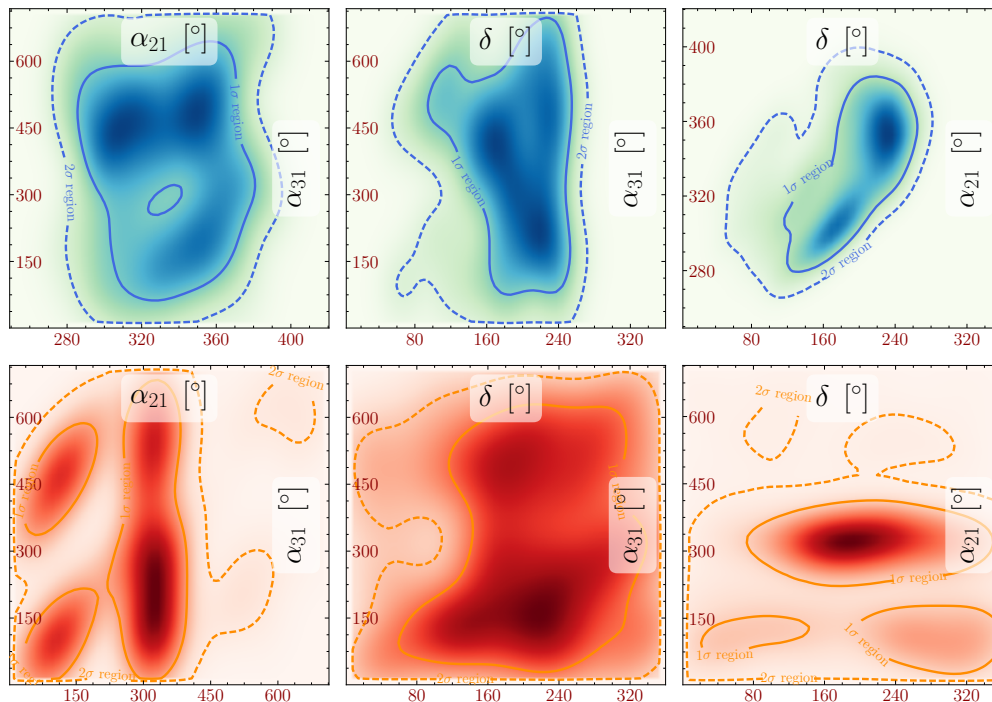
Figure 2. The two-dimensional projections for leptogenesis with $M_1 = 10^{10}$ GeV and CP violation provided only by the phases of the PMNS matrix. The NO case is coloured blue/green and the IO one is orange/red. The contours correspond to 68% and 95% confidence levels. This plot was created using SUPERPLOT [88].

fixed or constrained as stated, we explore the parameter space using a flat prior and log-likelihood function evaluated at a point $\mathbf{p} = (\delta, \alpha_{21}, \alpha_{31}, m_{1,3}, M_2, M_3)$ (varying m_1 or m_3 for normal or inverted ordering respectively) by

$$\log L = -\frac{1}{2} \left(\frac{\eta_B^2(\mathbf{p}) - \eta_{B_{\mathrm{CMB}}}^2}{\Delta \eta_{B_{\mathrm{CMB}}}^2} \right), \tag{3.1}$$

to define regions of 1σ and 2σ agreement with the observed value of the asymmetry. In addition we impose a bound on the sum of neutrino masses of 1 eV which is consistent with the tritium beta-decay experiments [92–94] but more conservative than recent constraints from Planck [80]. In the numerical work of this section we allow only for the two lightest heavy Majorana neutrinos to decay (an excellent approximation) and we neglect lepton number-changing scattering processes, spectator effects [20, 95], thermal corrections [96, 97] and the inclusion of quantum statistical factors [98–101] which typically introduces an $\mathcal{O}(10\%)$ error [27, 102–104]. To solve the density matrix equations we use the PYTHON interface [105] to the LSODA algorithm [106] that is available in SCIENTIFIC PYTHON [107]. Due to the high-dimensionality of the parameter space we found the use of MULTINEST [108–110] (more explicitly, PYMULTINEST [111], a wrapper around MULTINEST written in PYTHON) particularly useful. In figure 8 we display the two-dimensional posterior probability plots for the CP-violating PMNS phases in the normal ordered and inverted ordered cases.

δ	α_{21}	α_{31}	M_1	M_2	M_3	x_1	x_2	x_3	y_2
(°)	(°)	(°)	(GeV)	(GeV)	(GeV)	(°)	(°)	(°)	(°)
228	447	570	2.82×10^{10}	1.00×10^{13}	3.16×10^{13}	90	18	180	0

Table 2. A benchmark point for leptogenesis with $M_1 = 2.82 \times 10^{10}$ GeV, with normal ordering. Here, we have $m_1 = 0.02$ eV and $y_1 = y_3 = -33°$, corresponding to $\mathcal{F} = 0.27$. This point produces $\eta_B = 6.1 \times 10^{-10}$.

The results of this parameter search are shown in the form of two-dimensional projections in figure 2. For points in these regions of parameter space for which $\eta_B = \eta_{B_{\mathrm{CMB}}}$, the fine-tuning is $\mathcal{F} \approx 0.23$ which corresponds only to a very slight enhancement of the R-matrix. The values of lightest neutrino mass for NO (IO) neutrino mass spectrum corresponding to this case are $m_{1(3)} = 0.0215$ eV. For the best-fit values of the fitted parameters in the NO (IO) case we find: $\delta = 133.76°$ (139.8°), $\alpha_{21} = 315.5°$ (165.3°), $\alpha_{31} = 551.0°$ (565.5°), $M_2 = 4.90$ (4.97) $\times 10^{11}$ GeV, $M_3 = 2.19 \times 10^{12}$ GeV, $x_2 = 113.4°$ (13.9°). For the case of an NO light neutrino mass spectrum, we find that the observed baryon asymmetry may be obtained to within 1σ (2σ) with δ between $[95, 265]°$ ($[52, 282]°$). For IO, the 1σ (2σ) range is $[60, 338]°$ ($[8, 360]°$). Both of these scenarios comfortably incorporate the measured bounds on δ (table 1). In what follows, we provide some explanation of these results and plots by introducing an analytical approximation which we use to study the scenarios where only the Dirac or only the Majorana phases provide CP violation.

3.2 Dependence of η_B on the Dirac and Majorana phases

In the scenario $10^9 < M_1(\mathrm{GeV}) < 10^{12}$, it is appropriate to apply the two-flavour Boltzmann equations (eq. (2.46)). These equations have the following analytical solution [112]

$$n_{B-L} \approx \frac{\pi^2}{6z_d K_1} n_{N_1}^{\mathrm{eq}}(z_0) \left(\epsilon_{\tau\tau}^{(1)} \frac{1}{P_{\tau\tau}^{0(1)}} + \epsilon_{\tau^\perp\tau^\perp}^{(1)} \frac{1}{P_{\tau^\perp\tau^\perp}^{0(1)}} \right), \tag{3.2}$$

where it is assumed that the dominant contribution to the final asymmetry is from the lightest of the heavy Majorana neutrinos and that leptogenesis occurs in the strong washout regime. We denote the z for which the washout becomes less than one as z_d, $W(z_d) < 1$, $K_1 \equiv \Gamma_1/H(M_1)$ is the decay parameter for N_1, and the z for which leptogenesis is initiated as z_0. As we are interested in those scenarios in which CP violation derives only from the phases of the PMNS matrix, we have the supplementary condition $\mathrm{Tr}\, \epsilon^{(1)} = 0$ (or $\epsilon_{\tau\tau}^{(1)} = -\epsilon_{\tau^\perp\tau^\perp}^{(1)}$) which we may use to simplify the solution to

$$n_{B-L} = \frac{\pi^2}{6z_d K_1} n_{N_1}^{\mathrm{eq}}(z_0) \epsilon_{\tau\tau}^{(1)} \Delta F, \tag{3.3}$$

with

$$\Delta F \equiv \frac{1}{P_{\tau\tau}^{0(1)}} - \frac{1}{P_{\tau^\perp\tau^\perp}^{0(1)}} = \frac{1}{P_{\tau\tau}^{0(1)}} - \frac{1}{1 - P_{\tau\tau}^{0(1)}}. \tag{3.4}$$
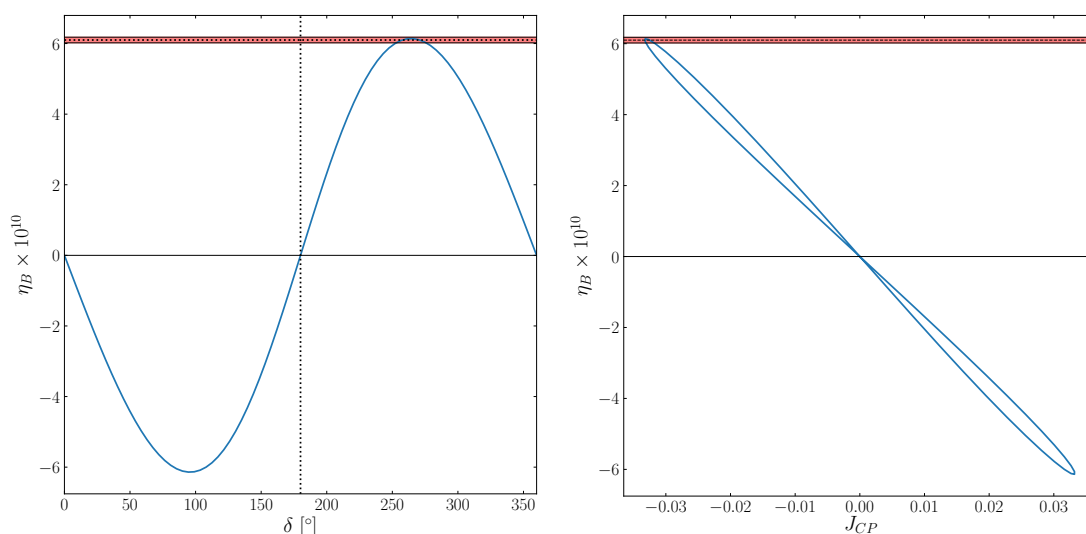
Figure 3. The baryon asymmetry with $M_1 = 5.13 \times 10^{10}$ GeV and CP violation provided solely by δ. The Majorana phases are fixed at $\alpha_{21} = 180°$ and $\alpha_{31} = 0°$. The red band indicates the 1σ observed values for $\eta_{B_{\mathrm{CMB}}}$ with the best-fit value indicated by the horizontal black dotted line. Left: the final baryon asymmetry as a function of δ with exact CP-invariance when $\delta = 0°$ and $180°$ (vertical black dotted line). Right: a parametric plot of η_B against J_{CP} as δ is varied. See the text for further details.
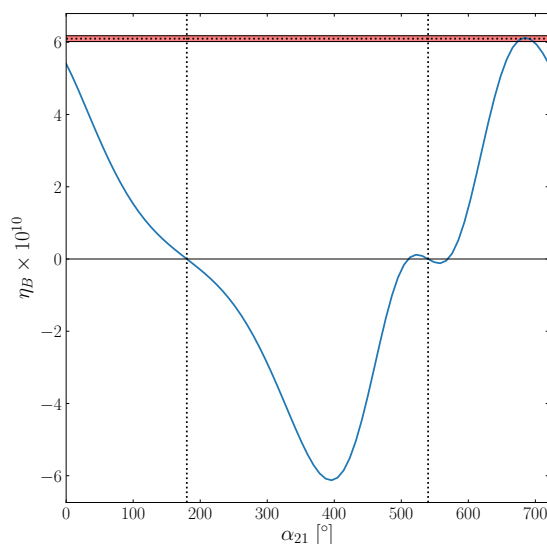

Figure 4. The baryon asymmetry with $M_1 = 3.05 \times 10^{10}$ GeV and CP violation provided solely by α_{21} (corresponding to $\delta = \alpha_{31} = 0°$). The red band indicates the 1σ observed values for η_B with the best-fit value indicated by the horizontal black dotted lines. Here we show the baryon asymmetry against α_{21} with exact CP-invariance at $\alpha_{21} = 180°$ and $540°$ (vertical black dotted lines).
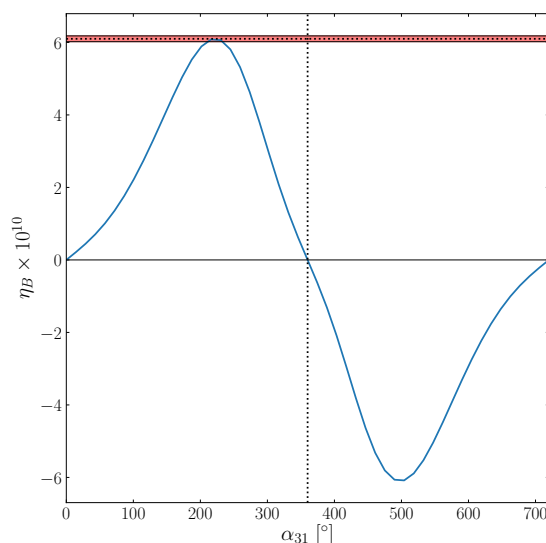
Figure 5. The baryon asymmetry with $M_1 = 5.13 \times 10^{10}$ GeV and CP violation provided solely by α_{31} (corresponding to $\delta = 0°$, $\alpha_{21} = 180°$). The red band indicates the 1σ observed values for η_B with the best-fit value indicated by the horizontal black dotted lines. Here we show the baryon asymmetry as a function of α_{31}, exact CP-invariance exists for $\alpha_{31} = 0°$ and $360°$ (vertical black dotted lines).

At the benchmark point for normal ordering defined in table 2, which we will use in the further analyses in the present section, we have:

$$Y_{\tau 1} = 1.37 \times 10^{-3} - 1.67 \times 10^{-4} e^{i\delta},$$
$$Y_{\tau 1} = 6.64 \times 10^{-4} - 8.74 \times 10^{-4} e^{i\frac{\alpha_{21}+\pi}{2}}, \qquad (3.5)$$
$$Y_{\tau 1} = 4.71 \times 10^{-4} + 1.07 \times 10^{-3} e^{\frac{i\alpha_{31}}{2}},$$

for CP violation from δ, α_{21} and α_{31} respectively. For the case in which δ provides the CP violation in eq. (3.5), this phase gives a subdominant contribution to $|Y_{\tau 1}|$. As can be shown, $P_{\tau\tau}^{0(1)}$ is similarly weakly dependent on the phases. Thus, the phase dependence of the solutions of eq. (3.3) does not come predominantly from the flavour factor ΔF but from the CP-asymmetry $\epsilon_{\tau\tau}^{(1)}$. However, in the case of α_{21} providing the CP violation, the two terms of eq. (3.5) are similar in magnitude and we may get a strong enhancement in ΔF. The final case where α_{31} provides the CP violation is intermediate and should experience a slight phase-dependent enhancement from ΔF.

3.2.1 Dirac phase CP violation

In this subsection, we consider deviations from the benchmark point of table 2 where we allow δ to vary but fix $\alpha_{21} = 180°$ and $\alpha_{31} = 0°$. Given the pattern of R-matrix angles, this ensures that any CP violation comes solely from δ. In this case, the $\tau\tau$-component of the CP-asymmetry is given by

$$\epsilon_{\tau\tau}^{(1)} = (0.515 - 3.94 c_{13}) s_{13} \times 10^{-8} \sin\delta = -0.501 \times 10^{-8} \sin\delta. \qquad (3.6)$$

Thus, given the approximate phase-independence of ΔF, we obtain a sinusoidal dependence of η_B on δ, with $\eta_B = 0$ when $\delta = 0°$ or $180°$. Keeping all other parameters fixed, we find that for $M_1 = 2.82 \times 10^{10}$ GeV no value of δ can produce the observed baryon asymmetry of the Universe, the maximum value of η_B as a function of δ is 4.07×10^{-11}. We might scale the heavy Majorana neutrino masses by a constant value, as when the two-flavour approximation of eq. (3.3) is valid, the factor $\epsilon_{\tau\tau}^{(1)}$ scales in proportion with this constant and thus so does η_B. In doing so, we find that the final asymmetry rises until $M_1 = 7.08 \times 10^{11}$ GeV, where η_B takes maximum value 4.01×10^{-10}. After this, the simple scaling fails as one begins to enter the transition to what is usually the single-flavour regime.

Performing a detailed numerical parameter exploration we find that purely Dirac phase CP violation leads to successful leptogenesis for $M_1 = 5.13 \times 10^{10}$ GeV, $M_2 = 2.19 \times 10^{12}$ GeV and $M_3 = 1.01 \times 10^{13}$ GeV. This is illustrated in figure 3 in which the plotted η_B comes from solving the full density matrix equations. In this case, we have:

$$Y_{\tau 1} = 1.11 \times 10^{-2} - 2.40 \times 10^{-4} e^{i\delta}. \tag{3.7}$$

Given the different order of magnitude of the two terms in the expression for $Y_{\tau 1}$, the baryon asymmetry should exhibit dependence on δ only from $\epsilon_{\tau\tau}^{(1)}$ and not from ΔF. Our theoretical expectations are borne out by the approximate sinusoidal dependence of η_B on δ seen in figure 3.

3.2.2 CP violation from the Majorana phase α_{21}

Here, we set $\delta = \alpha_{31} = 0°$ but allow CP violation from α_{21}. Setting all other parameters to their benchmark values we find

$$\epsilon_{\tau\tau}^{(1)} = 3.14 \times 10^{-7} \cos \frac{\alpha_{21}}{2}. \tag{3.8}$$

It follows from this expression for $\epsilon_{\tau\tau}^{(1)}$ that at the CP-conserving values for $\alpha_{21} = 0°, 360°$ we have $\epsilon_{\tau\tau}^{(1)} \neq 0$ (see also figure 4). This corresponds to the case of CP-conserving R-matrix, CP-conserving PMNS matrix, but CP-violating interplay between the R and PMNS matrix elements in leptogenesis [25]. In a similar way to the previous subsection, we find that no value of α_{21} can achieve successful leptogenesis using this combination of phases and the benchmark values from table 2. Thus, we find it necessary to scale all of the heavy Majorana neutrino masses by a common factor such that $M_1 = 3.05 \times 10^{10}$ GeV, may allow for successful leptogenesis. With this scaling we obtain the results plotted in figure 4. The deviation from pure (co)sinusoidal behaviour is explained by the α_{21}-dependence of ΔF. For $\alpha_{21} < 360°$, ΔF varies relatively slowly exhibiting a global minimum at $\alpha_{21} = 180°$, resulting in a slightly modified sinusoidal dependence through this point in η_B. A strong peak exists for ΔF around $\alpha_{21} = 540°$, which results in the peak of η_B occurring before $720°$, as would be expected from the dependence of $\epsilon_{\tau\tau}^{(1)}$. The small sign-changing fluctuation around the zero at $\alpha_{21} = 540°$ is a feature that does not appear in the solution of two-flavour Boltzmann equations and thus cannot be explained in terms of the analytic solution eq. (3.3). However, the extra zeros of η_B that are seen in figure 4 are due only to accidental cancellations and do not correspond to cases of CP-symmetry (unlike those at $\alpha_{21} = 180°$ and $\alpha_{21} = 540°$).
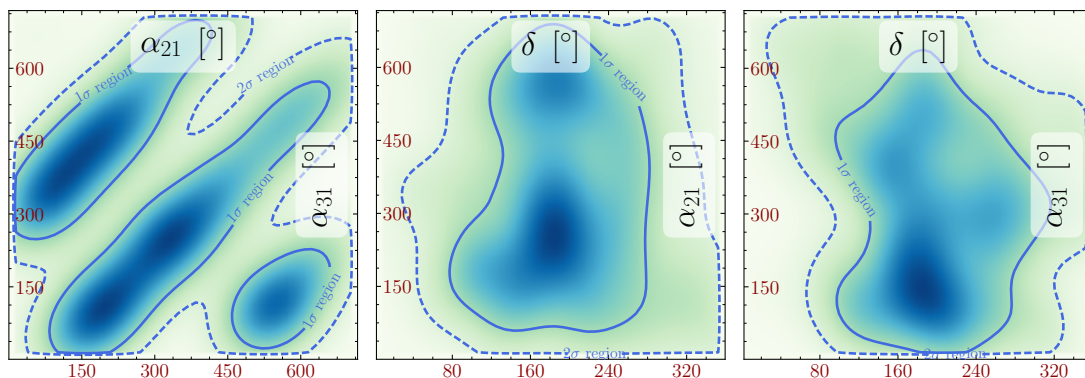
Figure 6. The two-dimensional projections for leptogenesis with $M_1 = 10^{11}$ GeV, $M_2 = 10^{12}$ GeV and N_3 decoupled, with CP violation provided only by the phases of the PMNS matrix. Here it is assumed that the light neutrino mass spectrum has normal ordering. Contours correspond to 68% and 95% confidence levels. This plot was created using SUPERPLOT [88].

3.2.3 CP violation from the Majorana phase α_{31}

We set $\delta = 0°$ and $\alpha_{21} = 180°$ such that CP violation is provided by α_{31}. Using the benchmark values for the other parameters from table 2 we find:

$$\epsilon_{\tau\tau}^{(1)} = 2.11 \times 10^{-7} \sin \frac{\alpha_{31}}{2}. \tag{3.9}$$

Again we find that without scaling the heavy Majorana neutrino masses, no value of α_{31} corresponds to successful leptogenesis. At $M_1 = 5.13 \times 10^{10}$ GeV we obtain the first point for which the observed baryon asymmetry is created and this is plotted in figure 5. We see that analytical expectation of a sinusoidal dependence of the baryon asymmetry ($\eta_B \propto \epsilon_{\tau\tau}^{(1)} \propto \sin(\alpha_{31}/2)$) from eq. (3.9) is present. ΔF exhibits a broad peak around $\alpha_{31} = 360°$ which results in the slight shift to the centre of the otherwise sinusoidal peaks.

3.3 The case of N_3 decoupled

In this section, we review the case that the heaviest Majorana neutrino, N_3, physically decouples. We restrict ourselves to normal ordered light neutrino masses. The resultant scenario with two relevant heavy Majorana neutrinos is the simplest (minimal) type I framework compatible with all neutrino data. In this scenario only two of the light neutrinos have non-zero masses since $m_1 = 0$. For normal ordering, the R-matrix may be parametrised as [113–115]

$$R = \begin{pmatrix} 0 & \cos\theta & \sin\theta \\ 0 & -\sin\theta & \cos\theta \\ 1 & 0 & 0 \end{pmatrix}. \tag{3.10}$$

The resulting neutrino Yukawa matrix thus has $Y_{\alpha 3} = 0$, consistent with the premise that N_3 has decoupled. We choose to take θ in eq. (3.10) to be real in order to have the condition of eq. (2.16) satisfied. We assume further that at least one of the three phases in the PMNS matrix has a CP-violating value.

As with the previous sections, we have performed an exhaustive exploration of the parameter space where again we are primarily concerned with the situation in which CP

δ	α_{21}	α_{31}	M_1	M_2	θ
(°)	(°)	(°)	(GeV)	(GeV)	(°)
228	516	100	10^{11}	10^{12}	25.05

Table 3. A benchmark point for leptogenesis with $M_1 = 10^{11}$ GeV and N_3 decoupled with a normal ordered light mass spectrum.

violation is provided only by the PMNS phases. We choose to fix $M_1 = 10^{11}$ GeV and $M_2 = 10^{12}$ GeV such that the parameter space to explore is described by $\mathbf{p} = (\delta, \alpha_{21}, \alpha_{31}, \theta)$. In figure 6, we present the two-dimensional posterior projection for the case of normal ordering. Here, it is seen that with $M_1 = 10^{11}$ GeV, for normal ordering, successful leptogenesis may produce a baryon asymmetry with 1σ (2σ) agreement with the observed value for $\delta \in [95, 315]°$, ($\delta \in [25, 360]°$).

In table 3, we provide a benchmark point for normal ordered leptogenesis, with purely low-energy CP violation and N_3 decoupled. At this point, the observed BAU is produced with a corresponding fine-tuning of $\mathcal{F} = 0.23$. In figure 7, we illustrate a similar scenario, in which the CP violation is provided only by δ ($\alpha_{21} = 180°$, $\alpha_{31} = 0°$), and where the observed baryon asymmetry is produced near $\delta = 270°$. We conclude that, even for the minimal type I seesaw scenario with two heavy Majorana neutrinos exhibiting hierarchical mass spectrum, it is possible to generate the observed value of the baryon asymmetry with the requisite CP violation provided exclusively by the Dirac phase δ, and/or by the Majorana phase α_{21} or α_{31}.

Furthermore, we note that, in performing a similar investigation for the inverted ordering scenario, we find no point in the parameter space which corresponds to successful leptogenesis with N_3 decoupled in this mass window[9] with real R-matrix. If, however, e.g., $R_{11}R_{12} = \pm i |R_{11}R_{12}|$ ($R_{13} = 0$ in the case of interest), we can have successful leptogenesis with the CP violation provided by the Dirac and/or Majorana phases in PMNS matrix also for the IO spectrum. These conclusions are in agreement with the results of [25] wherein one may find a detailed discussion of the cases considered in the present subsection.

Finally, in [25] the following necessary condition for successful leptogenesis in the case of NO spectrum with the requisite CP violation provided exclusively by the Dirac phase δ was obtained:

$$|\sin\theta_{13}\,\sin\delta| \gtrsim 0.09\,. \tag{3.11}$$

We recall that this condition was derived by using values of the the CP-conserving R-matrix elements maximising the lepton asymmetry and assuming that the transition from two-flavour to one-flavour regime starts at $T \cong 5 \times 10^{11}$ GeV, i.e., that at $M_1 \lesssim 5 \times 10^{11}$ GeV the two-flavour regime is fully effective.

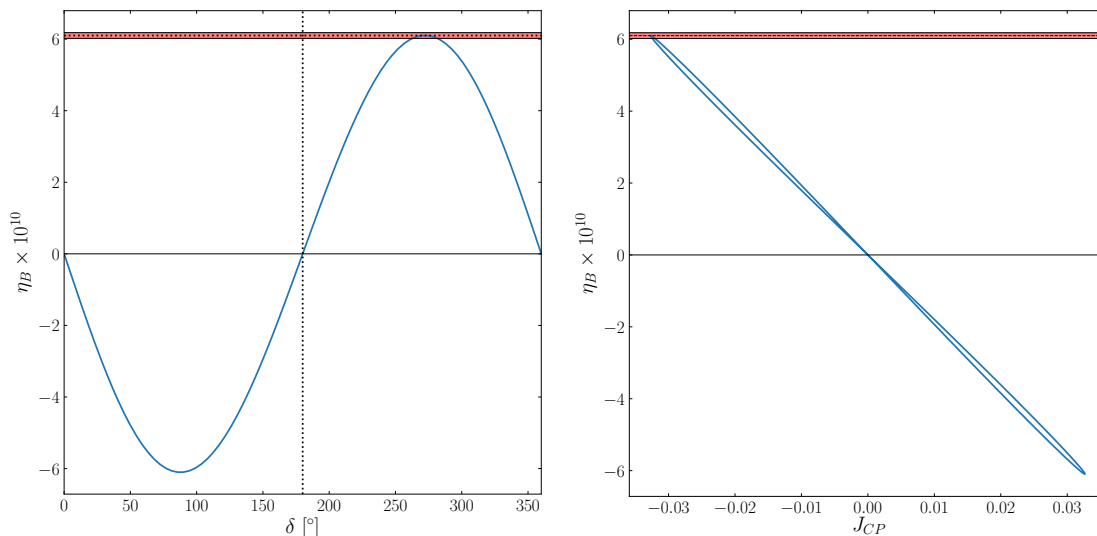[9]For IO light neutrino mass spectrum the decoupling of N_3 implies $R_{13} = 0$. In this case $m_3 = 0$ as well.

Figure 7. The baryon asymmetry from leptogenesis with $M_1 = 10^{11} \, \text{GeV}$ and N_3 decoupled, where CP violation is provided only by the Dirac phase δ. The red bands indicate the values in 1σ agreement with the observed value $\eta_{B_{\text{CMB}}}$. Left: a plot of η_B against δ, showing successful leptogenesis near the maximal CP-violating value $\delta = 270°$. Right: the corresponding parametric plot of η_B with J_{CP} as δ is varied. See the text for further details.

4 Leptogenesis in the regime $M_1 < 10^9$ GeV

Successful thermal leptogenesis at intermediate scales may be accomplished through the combination of flavour effects and fine-tuned Yukawa matrices with $\mathcal{F} \gtrsim \mathcal{O}(10)$ [78, 116]. In section 2.3, we first review these fine-tuned scenarios and then proceed to determine the subset among them in which the R-matrix is CP-conserving while the PMNS matrix contains CP-violating phases. In section 4.1 we present and analyse the results of a comprehensive search of the model parameter space for regions with successful leptogenesis compatible with these subsets where we have numerically solved the density matrix equations, for two-decaying heavy Majorana neutrinos, exactly. Following this, we consider in detail the scenarios in which CP violation is due solely to the Dirac phase in section 4.2.1, or due only to the Majorana phases in section 4.2.2 and section 4.2.3. In appendix B, we display results for $M_1 = 10^9$ GeV, where $\mathcal{O}(10)$ fine-tuning is also required.

We present an analytic approximation of the baryon asymmetry to find that the detailed dependence of the baryon asymmetry on the low energy phases may be roughly explained by the features of $Y_{\tau 1}$ and $Y_{\mu 1}$. We reiterate that we apply these approximation simply to illustrate the qualitative behaviour of the solutions but we numerically solve the density matrix to produce all plots in this paper.

4.1 Results of parameter exploration

The options of eq. (2.37) are satisfied by sixteen distinct R-matrices which may be divided into four classes according to the corresponding parity vectors ρ^ν, ρ^N (see appendix A for definitions and further details). All such matrices are identical except for the placement of factors ± 1 or $\pm i$. The phenomenological implications of each will be qualitatively similar
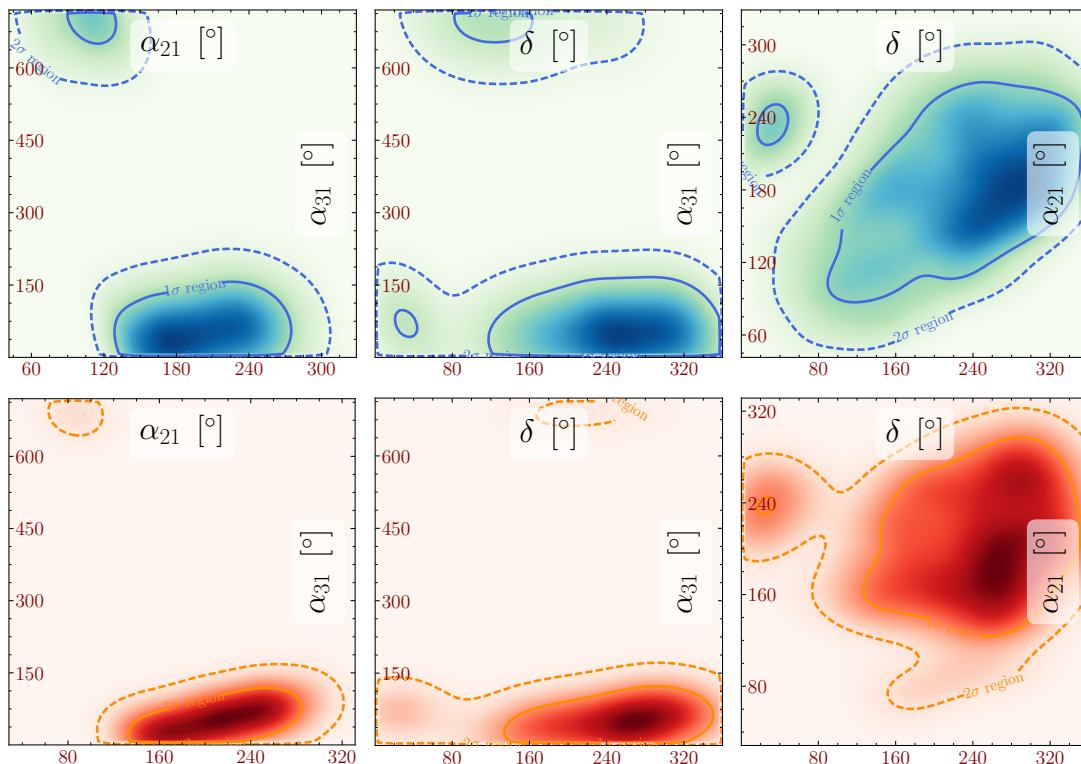
Figure 8. The two-dimensional projections for intermediate scale leptogenesis with $M_1 = 3.16 \times 10^6$ GeV for $x_1 = 0$, $y_2 = 0$, $x_3 = 180°$, $y_1 = y_2 = 180°$, with CP violation provided only by the phases of the PMNS matrix. The normal ordered case is coloured blue/green and inverted ordering orange/red and contours correspond to 68% and 95% confidence levels. This plot was created using SUPERPLOT [88].

except for the precise positions in parameter space that certain features occur. As we are primarily concerned with demonstrating the viability of leptogenesis with the $\mathcal{O}(100)$ fine-tuned Yukawa matrices (of the type in eq. (2.28)) then we shall focus our numerical efforts on just one possible R-matrix of the set of sixteen. Namely, we choose a scenario corresponding to $\cos x_1 = 0$, $\cos x_3 = -1$ such that $\rho^\nu = \pm(+1, -1, +1)^T$, $\rho^N = \pm(+1, +1, -1)^T$.

For the numerical analysis, we follow the same procedure outlined in section 3.1 with one additional constraint. At values of $\mathcal{F} \gtrsim 1000$, higher-order corrections to the light neutrino mass become important. For this reason we fix $y_1 = y_3 = 180°$ and thereby avoid these problematic regions of the model parameter space.

In the parameter searches of this section, we consider two cases, in one we fix $M_1 \sim 10^6$ GeV (figure 8) and in the other we fix $M_1 \sim 10^8$ GeV (figure 9). We note that $M_2 = 3.5 M_1$ and $M_3 = 3.5 M_2$ and $m_1 = 0.21$ eV.[10] This allows for a comparison of the effects of two different degrees of fine-tuning, with the former corresponding usually to $\mathcal{F} \sim 500$. This is close to the maximum fine-tuning (and correspondingly, the smallest non-resonant leptogenesis scale) for which second-order radiative corrections to the mass can be ignored [78].

---

[10]In appendix B, we demonstrate that one may lower m_1 as far as 0.05 eV and still have successful leptogenesis in a albeit rather constrained parameter space.
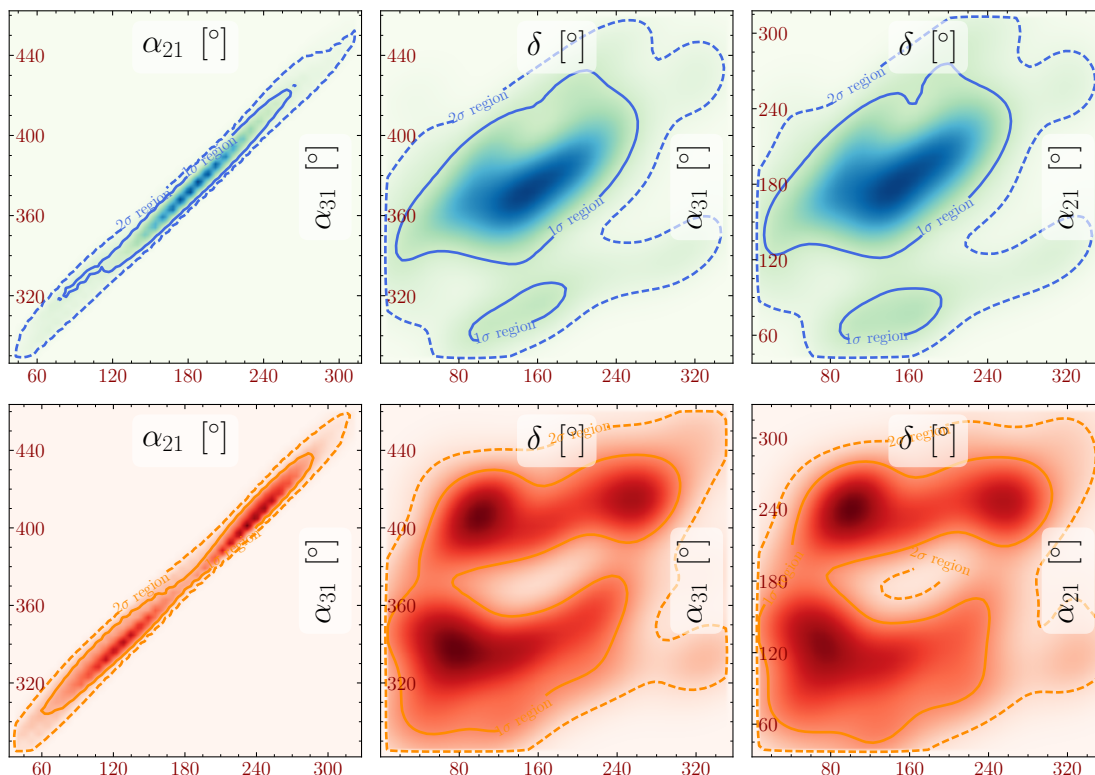
Figure 9. The two-dimensional projections for intermediate scale leptogenesis with $M_1 = 1.29 \times 10^8$ GeV for $x_1 = 0$, $y_2 = 0$, $x_3 = 180°$, $y_1 = y_2 = 180°$, with CP violation provided only by the phases of the PMNS matrix. The normal ordered case is coloured blue/green and inverted ordering orange/red and contours correspond to 68% and 95% confidence levels. This plot was created using SuperPlot [88].

For the scenario in which $M_1 = 3.16 \times 10^6$ GeV, as anticipated, there is a large fine-tuning of $\mathcal{F} = 745$. In the normal ordered case, we find that the observed baryon asymmetry may be obtained to within 1σ (2σ) with δ between $[84, 360]°$ ($[0, 360]°$). For inverted ordering, the 1σ (2σ) range is $[134, 350]°$ ($[0, 360]°$). With $M_1 = 1.29 \times 10^8$ GeV, the fine-tuning is considerably less, at $\mathcal{F} = 12$. In the normal ordered case, we find that the observed baryon asymmetry may be obtained to within 1σ (2σ) with δ between $[16, 263]°$ ($[0, 360]°$). For inverted ordering, the 1σ (2σ) range is $[0, 305]°$ ($[0, 360]°$). As in the previous section, we may explain these plots in detail by introducing an analytical approximation and the considering the simpler scenarios in which only the Dirac or only the Majorana phases provide CP violation. For brevity, we choose to perform this analysis only for $M_1 \sim 10^8$ GeV in the normal ordered scenario.

4.2 Dependence of η_B on Dirac and Majorana phases

In this section, we use the benchmark point given in table 4, in order to analytically study leptogenesis from low-energy CP violation in the case that the lightest heavy Majorana neutrino has mass $M_1 < 10^9$ GeV, such that a relatively high degree of fine-tuning in the light neutrino masses is required. We choose this benchmark point as it allows us to

δ	α_{21}	α_{31}	M_1	M_2	M_3	x_1	x_2	x_3	y_2
(°)	(°)	(°)	(GeV)	(GeV)	(GeV)	(°)	(°)	(°)	(°)
228	189	327.6	7.00×10^8	1.55×10^{10}	3.80×10^{10}	90	110	180	0

Table 4. A benchmark point for intermediate scale leptogenesis with quasi-degenerate (QD) spectrum of the light neutrino masses. In addition to the parameters listed we have $m_1 = 0.215\,\text{eV}$ and $y_1 = y_3 = -140°$ and corresponding fine-tuning $\mathcal{F} \approx 30$.
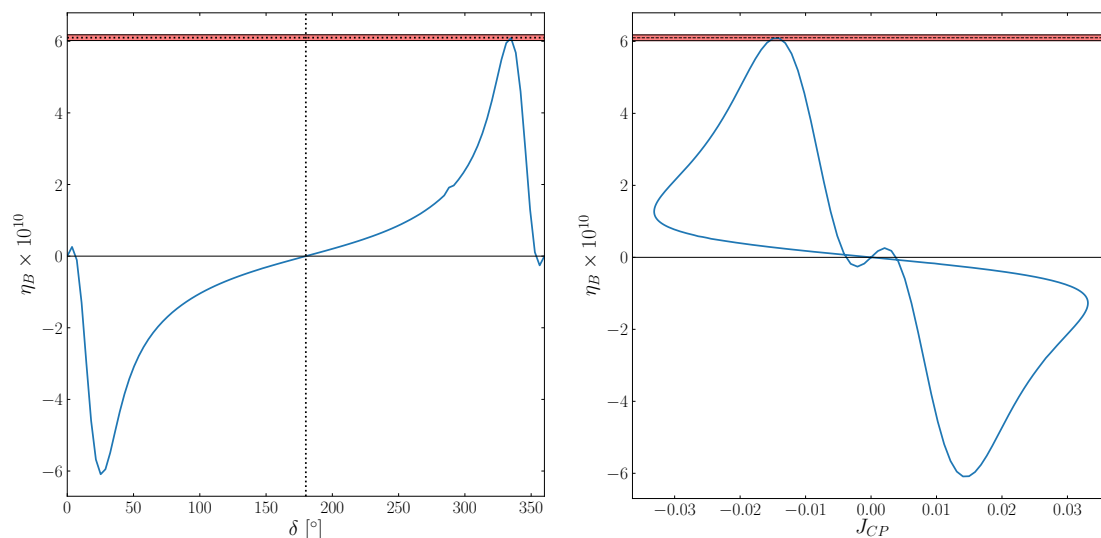

Figure 10. Intermediate scale leptogenesis ($M_1 = 7.00 \times 10^8$ GeV), with CP violation provided solely by δ, with $\alpha_{21} = 180°$ and $\alpha_{31} = 0°$. The red band indicates the 1σ observed values for $\eta_{B_{\text{CMB}}}$ with the best-fit value indicated by the horizontal black dotted line. Left: the final baryon asymmetry as a function of δ with exact CP-invariance when $\delta = 0°$ and $180°$ (vertical black dotted line). Right: a parametric plot of η_B against J_{CP} as δ is varied at intermediate scales ($M_1 = 7.00 \times 10^8$ GeV). See the text for further details.

accurately neglect the contributions from decays of the other heavy Majorana neutrinos and thus simplify the analysis.

With $M_1 < 10^9\,\text{GeV}$, leptogenesis occurs in the three-flavour regime for which the three-flavoured Boltzmann equations are a good approximation to the density matrix equations and have approximate analytical solution [112]:

$$n_{B-L} = \frac{\pi^2}{6 z_d K_1} n_{N_1}^{\text{eq}}(z_0) \left(\frac{\epsilon_{\tau\tau}^{(1)}}{P_{\tau\tau}^{0(1)}} + \frac{\epsilon_{\mu\mu}^{(1)}}{P_{\mu\mu}^{0(1)}} + \frac{\epsilon_{ee}^{(1)}}{P_{ee}^{0(1)}} \right), \tag{4.1}$$

where we take into account the decays of only the lightest heavy Majorana neutrino. As we are most interested in the scenarios in which CP violation is due to PMNS phases only, i.e. $\text{Tr}\,\epsilon^{(1)} = 0$, then we can re-express eq. (4.1) as

$$n_{B-L} = \frac{\pi^2}{6 z_d K_1} n_{N_1}^{\text{eq}}(z_0) \left(\epsilon_{\tau\tau}^{(1)} \Delta F_{\tau e} + \epsilon_{\mu\mu}^{(1)} \Delta F_{\mu e} \right), \tag{4.2}$$

where the asymmetry depends on the low-energy phases via $\epsilon_{\tau\tau}^{(1)}$ and $\epsilon_{\mu\mu}^{(1)}$ and from the

difference of the inverse flavour projections:

$$\Delta F_{\tau e} \equiv \frac{1}{P_{\tau\tau}^{0(1)}} - \frac{1}{P_{ee}^{0(1)}}, \quad \Delta F_{\mu e} \equiv \frac{1}{P_{\mu\mu}^{0(1)}} - \frac{1}{P_{ee}^{0(1)}}. \tag{4.3}$$

However, for the case of table 4, the two and three-flavour regime Boltzmann equations, to a high degree of accuracy give the same value of η_B. Given the comparative simplicity of the two-flavour solution eq. (3.3), we choose to use this for the practical purpose of simplifying the analysis.

For the benchmark parameter values listed in table 4, we may find analytical approximations for the CP-asymmetries $\epsilon_{\alpha\alpha}^{(1)}$. Under the relatively good approximation, that $m_1 = m_2$,[11] the asymmetry is given by

$$
\begin{aligned}
\epsilon_{\alpha\alpha}^{(1)} = &\frac{3}{16\pi (Y^\dagger Y)_{11}} \frac{M_1^2}{v^4} m_1 \sqrt{m_1 m_3} (e^{y_3} \sin 2x_2) |R_{21}|^2 \\
&\times \left(\frac{2}{3} \left(\frac{M_1}{M_2} + \frac{M_1}{M_3} \right) \Im \left[e^{-ix_3} (U_{\alpha 1} + i U_{\alpha 2}) U_{\alpha 3}^* \right] \right. \\
&\left. - \frac{5}{9} \frac{M_1^2}{M_2^2} \Im \left[e^{-2i(x_1 + x_3)} e^{-ix_3} (U_{\alpha 1} + i U_{\alpha 2}) U_{\alpha 3}^* \right] \right).
\end{aligned}
\tag{4.4}
$$

Selecting $x_1 = (2k_1 + 1)\pi/2$ and $x_3 = k_3\pi$ for $k_1, k_3 \in \mathbb{Z}$, such that $\cos x_1 = 0$ and $|\cos x_3| = 1$ and $\cos x_3 = (-1)^{k_3}$ is satisfied, we find the CP-asymmetry $\epsilon_{\alpha\alpha}^{(1)}$ to be

$$
\begin{aligned}
\epsilon_{\alpha\alpha}^{(1)} = &\frac{3}{16\pi (Y^\dagger Y)_{11}} \frac{M_1^2}{v^4} m_1^{\frac{3}{2}} m_3^{\frac{1}{2}} (e^{y_3} \sin 2x_2)(-1)^{k_3} |R_{21}|^2 \\
&\times \left(\frac{2}{3} \left(\frac{M_1}{M_2} + \frac{M_1}{M_3} \right) + \frac{5}{9} \frac{M_1^2}{M_2^2} \right) \Im \left[(U_{\alpha 1} + i U_{\alpha 2}) U_{\alpha 3}^* \right],
\end{aligned}
\tag{4.5}
$$

where, at our benchmark point, the coefficient of $\Im \left[U_{\alpha 3}^* (U_{\alpha 1} + i U_{\alpha 2}) \right]$ has magnitude approximately equal to 3.7×10^{-6}. This form is particularly useful in order to isolate the dependence of the CP-asymmetry on the PMNS phases in the factor $\Im \left[U_{\alpha 3}^* (U_{\alpha 1} + i U_{\alpha 2}) \right]$.

4.2.1 Dirac phase CP violation

We consider the possibility that the Majorana phases are CP-conserving: $\alpha_{21} = 180°$, $\alpha_{31} = 0°$ (given the R-matrix under consideration). The sole source of CP violation is δ and there is exact CP-invariance if $\delta = 0°, 180°$. The corresponding η_B is plotted in figure 10 alongside a parametric plot of η_B against $J_{\rm CP}$ with parameter δ.[12]

From the CP-asymmetry, one expects to find η_B proportional to

$$\Im \left[U_{\tau 3}^* (U_{\tau 1} + i U_{\tau 2}) \right] = s_{13} c_{13} c_{23}^2 (s_{12} - c_{12}) \sin \delta \approx -0.0178 \sin \delta, \tag{4.6}$$

and thus sinusoidal in δ. However, the phase-dependent efficiency (flavour-factor) ΔF exhibits a sharp maximum around the region $\delta = 0°$ or $\delta = 360°$. This modifies the

---

[11]The approximation $m_1 = m_2$ is sufficiently precise as long as $m_1^2 \gg 0.5\Delta m_{21}^2 \cong 3.7 \times 10^{-5}$ eV^2.

[12]All plots involving η_B in this work have been obtain by solving the full density matrix equations, allowing for the lightest pair of heavy Majorana neutrinos to decay and possibly (if indicated) include scattering effects.
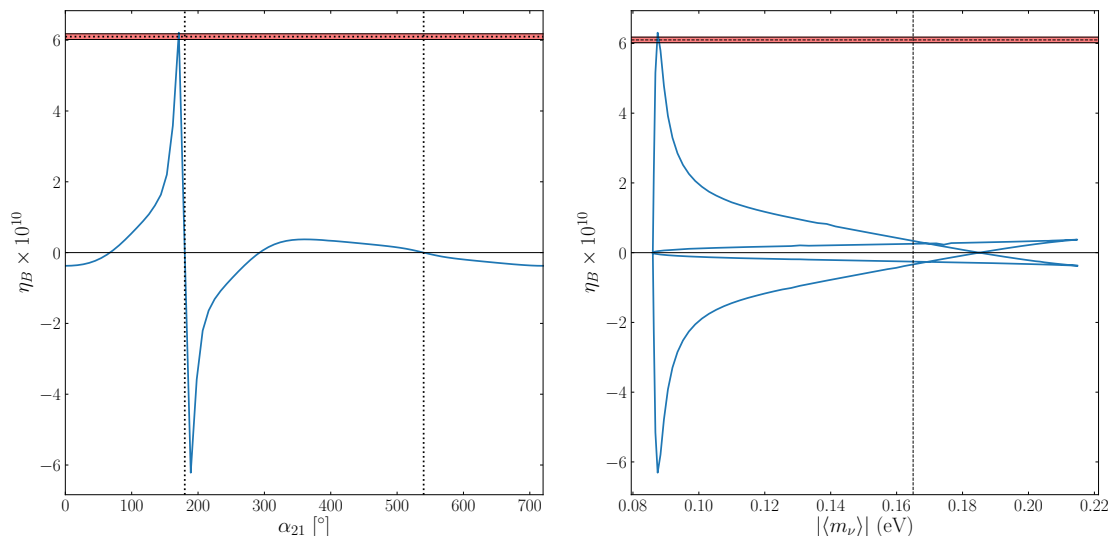
Figure 11. Intermediate scale leptogenesis ($M_1 = 7.00 \times 10^8 \,\mathrm{GeV}$) with CP violation provided solely by α_{21} and with $\delta = \alpha_{31} = 0$. The red band indicates the 1σ observed values for η_B with the best-fit value indicated by the horizontal black dotted lines. Left: the baryon asymmetry against α_{21} with exact CP-invariance at $\alpha_{21} = 180°$ and $540°$ (vertical black dotted lines). Right: a parametric plot of η_B against the effective neutrino mass $|\langle m_\nu \rangle|$ as α_{21} is varied with the vertical dashed black line denoting the upper value of the KamLAND-Zen bound 0.165 eV [74]. Successful leptogenesis is achieved for $|\langle m_\nu \rangle| = 0.0877\,\mathrm{eV}$. See the text for further details.

sinusoidal dependence from the CP-asymmetries such that the extrema of η_B are shifted towards the extreme values of δ, as in seen in figure 10. The small fluctuations around $\delta = 0°$, $\delta = 360°$ are not captured by the Boltzmann equations (neither two-flavoured nor three-flavoured) and are only present when solving the full density matrix equations which take account of the finite size of the lepton thermal widths. The result is the addition of some accidental zeros in the variation η_B which do not correspond to CP-conserving values of δ.

4.2.2 CP violation from the Majorana phase α_{21}

Alternatively, consider the case of CP violation from α_{21}, where $\delta = 0°$, $\alpha_{31} = 0°$ and all other parameters are set to their benchmark values of table 4. The variation of η_B with α_{21} in this scenario is plotted on the left of figure 11. On the right of the same figure, we parametrically plot η_B against $|\langle m_\nu \rangle|$ with parameter α_{21}. The baryon asymmetry η_B vanishes at the CP-conserving values of $\alpha_{21} = 180°$ and $540°$. However, as is seen in figure 11, $\eta_B \neq 0$ at the CP-conserving values of $\alpha_{21} = 0°$, $360°$ and $720°$ since at these values the interplay between the CP-conserving R and PMNS matrices leads to CP violation in leptogenesis [25].

The efficiency function ΔF, when plotted as a function of α_{21}, exhibits a very strong narrow peak at $\alpha_{21} = 180°$ and a much less pronounced peak at $\alpha_{21} = 540°$. As a consequence, the corresponding η_B is modified from the simple cosine curve expected from
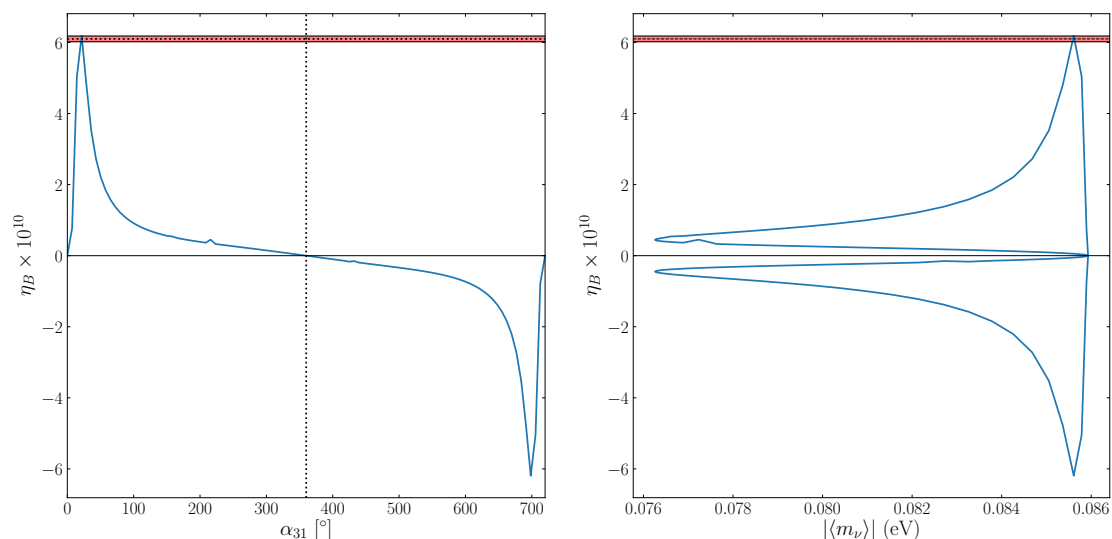
Figure 12. Leptogenesis at intermediate scales ($M_1 = 7.00 \times 10^8 \,\mathrm{GeV}$) when CP violation is provided solely by α_{31} with $\delta = 0°$, $\alpha_{21} = 180°$. The red band indicates the 1σ observed values for η_B with the best-fit value indicated by the horizontal black dotted lines. Left: the baryon asymmetry as a function of α_{31}. Exact CP-invariance exists for $\alpha_{31} = 180°$ and $360°$ (vertical black dotted lines). Right: a parametric plot of η_B against the effective neutrino mass $|\langle m_\nu \rangle|$ as α_{31} is varied with successful leptogenesis at $|\langle m_\nu \rangle| = 0.0856 \,\mathrm{eV}$. See the text for further details.

the dependence of $\epsilon_{\tau\tau}^{(1)}$ and $\epsilon_{\mu\mu}^{(1)}$ on α_{21}, which arises in the factors:

$$\Im\left[U_{\tau 3}^* \left(U_{\tau 1} + iU_{\tau 2}\right)\right] = -c_{13}c_{23}(c_{12}s_{23} + s_{12}c_{23}s_{13})\cos\frac{\alpha_{21}}{2} \approx -0.444\cos\frac{\alpha_{21}}{2}, \qquad (4.7)$$

Thus, there is a sharp transition around $\alpha_{21} = 180°$. We can conclude then that the strong peak in ΔF is what has allowed the observed baryon asymmetry of the Universe to be reproduced. This peak originates in an accidental cancellation of terms in the function $P_{\tau\tau}^{0(1)}$. There is no *a priori* reason to expect such a cancellation and it should be understood as a feature of the fine-tuned solutions that are being here studied. Thus, we see that the flavour-effects introduce a pair of accidental zeros of η_B, one in the range $[180, 540]°$ and the other in $[0, 180]°$.

4.2.3 CP violation from the Majorana phase α_{31}

Finally, consider the case of CP violation from α_{31} where $\delta = 0°$, $\alpha_{21} = 180°$ and for which the baryon asymmetry is plotted in the left plot of figure 12 and on the right we show the parametric dependence of the effective neutrino mass $|\langle m_\nu \rangle|$ with α_{31} against that of η_B. The baryon asymmetry η_B vanishes at the CP-conserving values of $\alpha_{31} = 0°$, $360°$ and $720°$.

The efficiency function ΔF in this case is qualitatively similar to that for the case of δ: CP violation only strongly peaks at α_{31} close to $0°$ and to $720°$. Thus, we do not observe, in the left plot of figure 12, the simple dependence, $\eta_B \propto \sin(\alpha_{31}/2)$ as may be expected

from the expression for $\epsilon_{\tau\tau}$,

$$\Im\left[U_{\tau 3}^*\left(U_{\tau 1}+iU_{\tau 2}\right)\right] = c_{13}c_{23}((c_{12}-s_{12})s_{23}+(c_{12}+s_{12})s_{13}c_{23})\sin\frac{\alpha_{31}}{2} \approx -0.662\sin\frac{\alpha_{31}}{2}. \tag{4.8}$$

Rather, we find an enhanced positive peak near $\alpha_{31} = 0°$ and an enhanced negative peak near $\alpha_{31} = 720°$.

4.2.4 Summary of fine-tuned solutions with high energy CP-symmetry

The fine-tuned solutions we have discussed in this section share the property that they enhance η_B through the production of a peak in the efficiency factor ΔF. In each projection coefficient,

$$P_{\alpha\alpha}^{0(1)} = \frac{|Y_{\alpha 1}|^2}{(Y^\dagger Y)_{11}}, \tag{4.9}$$

the PMNS matrix cancels from the denominator such that all phase-dependence comes from that of $|Y_{\alpha 1}|^2$ in the numerator. In this subsection, we may safely use the usual Casas-Ibarra parametrisation (obtained by the replacement of f with $\sqrt{M^{-1}}$ in eq. (2.10)), to obtain

$$Y_{\alpha 1} = \sqrt{M_1}\left(\sqrt{m_1}R_{11}U_{\alpha 1}+\sqrt{m_2}R_{12}U_{\alpha 2}+\sqrt{m_3}R_{13}U_{\alpha 3}\right). \tag{4.10}$$

The absolute value $|Y_{\alpha 1}|$ is extremised when each term in the parentheses in eq. (4.10) has a common complex phase or when terms may differ in complex phase by π. This occurs at CP-conserving values of the PMNS phases and so the enhancement expected in the functions ΔF is likely to occur at CP-conserving phases also. As an example, around the benchmark point of table 4, we find that with only α_{21} contributing to CP violation ($\delta = \alpha_{31} = 0°$),

$$Y_{\tau 1} = \left(2.16 + 2.23e^{i\frac{\alpha_{21}+\pi}{2}}\right)\times 10^{-3}. \tag{4.11}$$

The absolute value of this function has extrema when $\alpha_{21} = 180°$ or $\alpha_{21} = 540°$ - the CP-conserving values. Moreover, the cancellation that occurs at $\alpha_{21} = 180°$ is strong because of the similarity in magnitude of the two terms in eq. (4.11). As a result of this there are strong peaks in ΔF which enhance η_B.

This is a way in which the solutions are found to be fine-tuned as there is no reason to expect these two terms to be so similar in size. At these same points, the asymmetries $\epsilon_{\alpha\alpha}^{(1)}$ are vanishing as CP is a symmetry in the leptonic sector. Thus η_B, being proportional to the product of $\epsilon_{\tau\tau}^{(1)}$ and ΔF, is strongly enhanced on either side of the CP-invariant points (for instance, around $\alpha_{21} = 180°$ in the left plot of figure 11). Thus the fine-tuned solutions tend to achieve large η_B of one-sign on one side of a CP-invariant point and large η_B of the opposite sign on the other side. Similarly, this effect persists when all phases may contribute together to CP violation (figure 8 and figure 9). Thus, successful leptogenesis tends to occur near $\alpha_{21} \sim 180°$, $\alpha_{31} \sim 0°$, $720°$ when leptogenesis is achieved with fine-tuned light neutrino masses, as it is at intermediate scales ($M_1 \lesssim 10^9\,\mathrm{GeV}$). Note that although we made these arguments based on the two-flavoured Boltzmann equations, very similar conclusions are reached based on considerations of $\Delta F_{\tau e}$ and $\Delta F_{\mu e}$ for the

solutions of the three-flavoured Boltzmann equations. For this reason, one expects similar behaviour to hold even for lower values M_1 such as in figure 8.

Furthermore, one may usually argue that Dirac-phase leptogenesis suffers a suppression not present in Majorana phase leptogenesis due to the factors of s_{13} that appear in the CP-asymmetries as shown in eq. (4.6). However, for Dirac-phase leptogenesis $\eta_B \propto \sin\delta\Delta F(\delta)$, where the maximum absolute value of $\Delta F(\delta)$ is ~ 408, whereas for α_{21} leptogenesis, $\eta_B \propto \cos\frac{\alpha_{21}}{2}\Delta F(\alpha_{21})$ with maximum absolute value ~ 77. Thus, what is more relevant when leptogenesis occurs intermediate scales, is the degree of enhancement from ΔF that occurs due to fine-tuning.

Finally, as we observe in figure 9, the contours for α_{21}, α_{31} show a strong dependence on $\alpha_{31} - \alpha_{21}$. A rough explanation of this is given by the dependence of $\epsilon_{\tau\tau}^{(1)}$ on the Majorana phases. With δ fixed at its benchmark value, but α_{21} and α_{31} free to vary, this CP-asymmetry is given by

$$\epsilon_{\tau\tau}^{(1)} \approx \left(1.46\cos\frac{(\alpha_{31} - \alpha_{21})}{2} + 0.869\sin\frac{\alpha_{31}}{2}\right) \times 10^{-7}, \qquad (4.12)$$

which exhibits a slightly dominant, $(\alpha_{31} - \alpha_{21})$-dependent contribution. This contribution is maximised when $\alpha_{31} = \alpha_{21}$.

5 Leptogenesis in the regime $M_1 > 10^{12}$ GeV

In previous studies in which a connection between low-energy CP violation (CP-conserving R) and leptogenesis was established [26], the scale of leptogenesis was limited to $M_1 \leq 5 \times 10^{11}$ GeV. This allowed for the use of the two-flavour Boltzmann equations as shown in eq. (2.46) where the CP-asymmetries $\epsilon_{\tau\tau}^{(1)}$ and $\epsilon_{\tau^\perp\tau^\perp}^{(1)}$ appear separately. The expectation had been that for $M_1 \gg 10^{12}$ GeV, the single-flavour Boltzmann equation eq. (2.41) would be appropriate. In this equation, the CP-asymmetries appear only in the factor $\text{Tr}\,\epsilon^{(1)} = 0$ and hence no baryon asymmetry may be produced. In section 5.1 we argue that even at high scales $M_1 \gg 10^{12}$ GeV, if R is CP-conserving, then flavour effects are significant and that the density matrix equations do not reduce to the single flavour Boltzmann equations. Hence we conclude that viable leptogenesis may result from low energy CP violation. Finally, in section 5.2 we proceed to numerically analyse this possibility in detail.

5.1 Flavour effects with $M_1 \gg 10^{12}$ GeV and high energy CP-symmetry

In appendix C, we demonstrate that the complete formal solution of the density matrix equations (eq. (2.49)), with one decaying heavy Majorana neutrino is

$$n_{B-L}(z_f) = \int_{z_0}^{z_f} e^{-\int_{z'}^{z_f} W_1(z'')dz''}\left(\text{Tr}\,\epsilon^{(1)}D_1(z')(n_{N_1}(z') - n_{N_1}^{\text{eq}}(z')) + W_1(z')\lambda(z')\right)dz', \qquad (5.1)$$

with

$$\lambda(z) \equiv 2\int_{z_0}^{z} dz'\Re\left[C_{1\tau^\perp}C_{1\tau}^*\frac{\Im(\Lambda_\tau)}{Hz'}n_{\tau\tau^\perp}(z')\right]. \qquad (5.2)$$
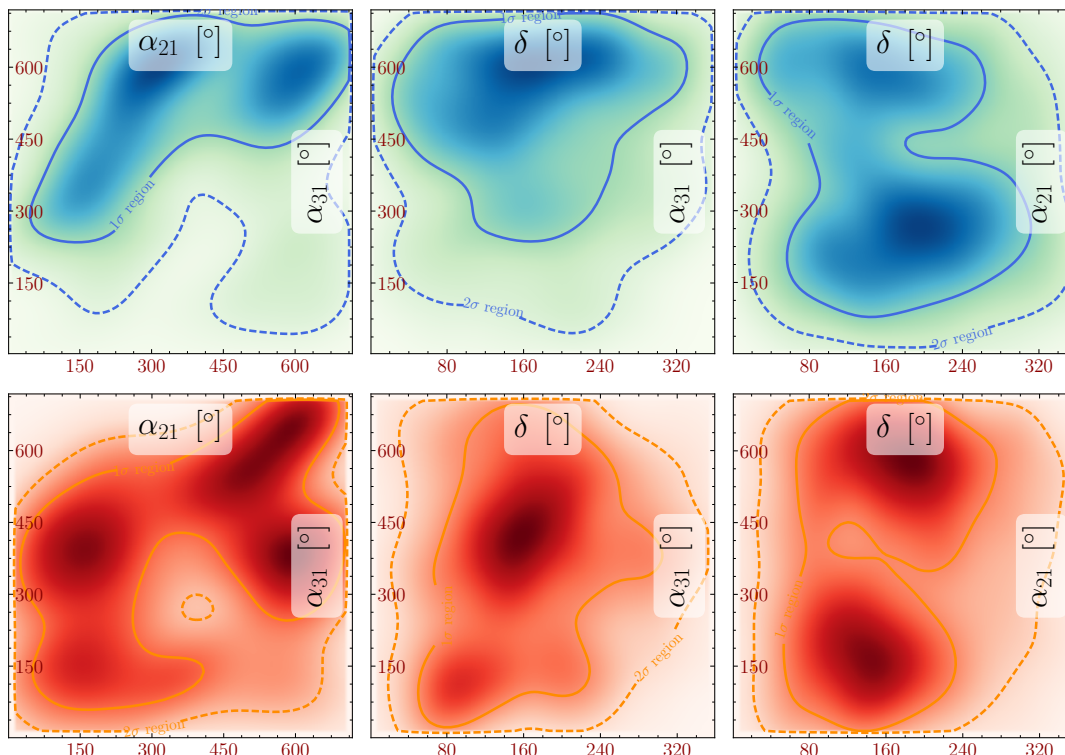
Figure 13. The two-dimensional projections for high-scale leptogenesis with $M_1 = 10^{13}$ GeV with CP violation provided only by the phases of the PMNS matrix. The NO case is coloured blue/green and the IO one is orange/red. The contours correspond to 68% and 95% confidence levels. This plot was created using SUPERPLOT [88].

In a typical leptogenesis scenario, if $M_1 \gg 10^{12}$ GeV, flavour effects are negligible and one obtains the well-known result:

$$n_{B-L}(z_f) = \int_{z_0}^{z_f} e^{- \int_{z'}^{z_f} W_1(z'') dz''} \operatorname{Tr} \epsilon^{(1)} D_1(z')(n_{N_1}(z') - n_{N_1}^{\text{eq}}(z')) dz', \qquad (5.3)$$

which may be found by solving the single flavour Boltzmann equation. However, with a CP-conserving R-matrix, such that CP violation is provided solely by the PMNS phases, one has $\operatorname{Tr} \epsilon^{(1)} = 0$ and so the λ term in eq. (5.1) becomes the dominant one:

$$n_{B-L}(z_f) = \int_{z_0}^{z_f} e^{- \int_{z'}^{z_f} W_1(z'') dz''} W_1(z') \lambda(z') dz'. \qquad (5.4)$$

If this is the case, then the baryon asymmetry is produced purely through flavour-effects from $\Im(\Lambda_\tau)/Hz$.

The physical effect of $\operatorname{Tr} \epsilon^{(1)} = 0$ is that opposite asymmetries are produced in the τ and $\tau^\perp$ flavours due to the decay of N_1: $\epsilon_{\tau\tau}^{(1)} = -\epsilon_{\tau^\perp\tau^\perp}^{(1)}$. However, with flavour effects, the lepton asymmetries $\epsilon_{\tau\tau}^{(1)}$ and $\epsilon_{\tau^\perp\tau^\perp}^{(1)}$ produced in the decay experience differing washouts such that $n_{\tau\tau} \neq -n_{\tau^\perp\tau^\perp}$ and $n_B = n_{\tau\tau} + n_{\tau^\perp\tau^\perp} \neq 0$. It is an asymmetry produced by this method that is described in eq. (5.4). The obvious question at this point is whether this can ever be large enough to produce the observed baryon asymmetry when $M_1 \gg 10^{12}$ GeV.

δ	α_{21}	α_{31}	M_1	M_2	M_3	x_1	x_2	x_3
(°)	(°)	(°)	(GeV)	(GeV)	(GeV)	(°)	(°)	(°)
228	200	175	10^{13}	1.2×10^{15}	10^{16}	-96.55	-105.2	141.4

Table 5. The benchmark values for high-scale leptogenesis with normal ordering. Here we have $m_1 = 0.0159\,\text{eV}$ and $y_1 = y_2 = y_3 = 0°$.

The density matrix equations may be conveniently expressed in terms of the vectors

$$\boldsymbol{n} \equiv (n_{\tau^\perp \tau^\perp}, n_{\tau\tau^\perp}, n_{\tau^\perp \tau}, n_{\tau\tau})^T, \tag{5.5}$$

$$\boldsymbol{\epsilon^{(1)}} \equiv (\epsilon^{(1)}_{\tau^\perp \tau^\perp}, \epsilon^{(1)}_{\tau\tau^\perp}, \epsilon^{(1)}_{\tau^\perp \tau}, \epsilon^{(1)}_{\tau\tau})^T, \tag{5.6}$$

as

$$\frac{d\boldsymbol{n}}{dz} = \boldsymbol{\epsilon^{(1)}} D_1 \left(n_{N_1} - n_{N_1}^{\text{eq}} \right) - \frac{1}{2}\mathcal{W}_1 \boldsymbol{n} - \frac{\Im(\Lambda_\tau)}{Hz}\mathcal{I}\boldsymbol{n}, \tag{5.7}$$

where

$$\mathcal{W}_1 \equiv W_1 \begin{pmatrix} 2|C_{1\tau^\perp}|^2 & C_{1\tau}^* C_{1\tau^\perp} & C_{1\tau} C_{1\tau^\perp}^* & 0 \\ C_{1\tau} C_{1\tau^\perp}^* & 0 & 1 & C_{1\tau} C_{1\tau^\perp}^* \\ C_{1\tau}^* C_{1\tau^\perp} & 0 & 1 & C_{1\tau}^* C_{1\tau^\perp} \\ 0 & C_{1\tau}^* C_{1\tau^\perp} & C_{1\tau} C_{1\tau^\perp}^* & 2|C_{1\tau^\perp}|^2 \end{pmatrix} \quad \text{and} \quad \mathcal{I} \equiv \begin{pmatrix} 0 & 0 & 0 & 0 \\ 0 & 1 & 0 & 0 \\ 0 & 0 & 1 & 0 \\ 0 & 0 & 0 & 0 \end{pmatrix}. \tag{5.8}$$

In terms of these quantities, the formal solution, with flavour effects neglected is:

$$\boldsymbol{n}(z_f) = \int_{z_0}^{z_f} e^{\int_{z'}^{z_f} \frac{1}{2}\mathcal{W}_1(z'')dz''} \boldsymbol{\epsilon^{(1)}} D(z')(n_{N_1}(z') - n_{N_1}^{\text{eq}}(z'))dz'. \tag{5.9}$$

Although flavour effects in high-scale leptogenesis may be negligible, this solution may not be accurately applied for finding η_B in the case that $\text{Tr}\,\epsilon^{(1)} = 0$. This is because there is a strong cancellation of components of the density matrix when computing $\eta_B = n_{\tau^\perp \tau^\perp} + n_{\tau\tau}$, such that the errors made in neglecting flavour effects are dominant. For this reason, we make use of it only for finding the approximate behaviour of individual components of the density matrix and avoid applying it to situations where this cancellation occurs.

If the heavy Majorana neutrino masses M_i are scaled by a common factor x, such that $M_i \to xM_i$, then: $\epsilon^{(1)}$ scales in proportion with x, D_1 and W_1 do not scale with x and $\Im(\Lambda_\tau)/Hz$ varies inversely with x. Consequently, according to eq. (5.9), $n_{\alpha\beta}(z)$ scales in proportion to x, (with increasing precision for larger x since we can better neglect the thermal widths). In λ the scaling of $\Im(\Lambda_\tau)/Hz$ cancels that of $n_{\tau\tau^\perp}$ and so λ does not scale with x if $M_1 \gg 10^{12}$ GeV. Thus, at sufficiently large values of M_1, η_B, given by eq. (5.4), asymptotically approaches a non-zero constant. This is shown in figure 14 (d) over a range of M_1 values in which the ratios M_1/M_2 and M_2/M_3 are fixed. The curve increases ever more slowly for larger M_1 as the approximation leading to eq. (5.9) becomes ever more precise. This may be interpreted as the transition region between the two flavour regime and the single flavour having grown infinitely large.[13] In each of the plots of figure 14, we see a

---

[13]If, contrary to our scenario of interest, R is CP-violating ($\text{Tr}\,\epsilon^{(1)} \neq 0$), then the first term in parantheses of eq. (5.1) eventually dominates the second for sufficiently large x and the single flavour regime is entered.

dip in the density matrix solution curve near 10^{12} GeV. This feature is due to the difference in sign of the two-flavour solutions, for which $\eta_B \propto \epsilon_{\tau\tau}^{(1)}/P_{\tau\tau}^{0(1)} + \epsilon_{\tau^\perp\tau^\perp}^{(1)}/P_{\tau^\perp\tau^\perp}^{0(1)} = 3.99 \times 10^{-4}$, compared to that of the single flavour solutions, where $\eta_B \propto \epsilon_{\tau\tau}^{(1)} + \epsilon_{\tau^\perp\tau^\perp}^{(1)} = -7.5 \times 10^{-6}$ (where these numbers are valid for plot (a) of figure 14 corresponding to CP-violating R-matrix). The dip appears as a result of plotting the absolute value of η_B on a logarithmic scale when η_B passes through zero during the transition between these regimes.

In appendix D, we discuss the robustness of the plateau that forms for large heavy Majorana neutrino masses when the effects of scattering and when a more realistic treatment of the right-handed taus are incorporated. In the next section we explore the parameter space of the three heavy Majorana neutrino type I seesaw with regard to the solutions of eq. (D.1) with CP-conserving R-matrix and $M_1 \gg 10^{12}$ GeV.

5.2 Results of parameter exploration

At values of $M_1 \gg 10^{12}$ GeV, fine-tuning through large elements of the R-matrix is not required for successful leptogenesis (if Majorana phases are allowed to play a role, otherwise large fine-tuning is required if only Dirac phases take effect). Thus, in this section we analyse the parameter space corresponding to real, and therefore CP-conserving, R-matrices ($y_i = 0°$), using the same numerical technique as described in section 4.1. In order to perform this analysis we fix $M_1 = 10^{13}$ GeV and again require $M_3 > 3M_2 > 9M_1$ in order to avoid the resonant regime. With a much higher value of M_1, one would need a correspondingly a higher temperature of inflation. For this reason, we choose to illustrate the possibility of successful thermal leptogenesis at just one order of magnitude beyond the two-flavour to single-flavour transition temperature of 10^{12} GeV. In figure 13, we display the two-dimensional projection plots for both normal ordering and inverted ordering.

In the NO case, we find that the observed baryon asymmetry may be obtained to within 1σ (2σ) with δ between $[240, 331]°$ ($[0, 360]°$). In the IO one, the 1σ (2σ) range is $[50, 304]°$ ($[20, 352]°$). In what follows, we analyse these results by considering separately the cases of purely Dirac or purely Majorana CP violation. For brevity we consider only the case of NO spectrum.

5.3 Dependence of η_B on the Dirac and Majorana phases

As the final value of the baryon asymmetry becomes approximately constant for $M_1 \gg 10^{12}$ GeV (see figure 14) with a CP-conserving R-matrix, then one can can use the value of η_B that is predicted by the two-flavour Boltzmann equations (2FBE) at the start of the transition $M_1 \sim 10^{12}$ GeV as a proxy for the full solution of the density matrix equations (DME). That is,

$$\eta_B^{\mathrm{DME}}\left(M_1 \gg 10^{12} \text{ GeV}\right) \approx \eta_B^{\mathrm{2FBE}}\left(M_1 \sim 10^{12} \text{ GeV}\right), \tag{5.10}$$

provided that the ratios M_2/M_1 and M_3/M_1 are fixed. This has the advantage that we may again make use of the result in eq. (3.3)

$$n_{B-L} \approx n_B^{\mathrm{2FBE}}\left(M_1 \sim 10^{12} \text{ GeV}\right) = \frac{\pi^2}{6z_d K_1} n_{N_1}^{\mathrm{eq}}(z_0)\epsilon_{\tau\tau}^{(1)}\Delta F, \tag{5.11}$$

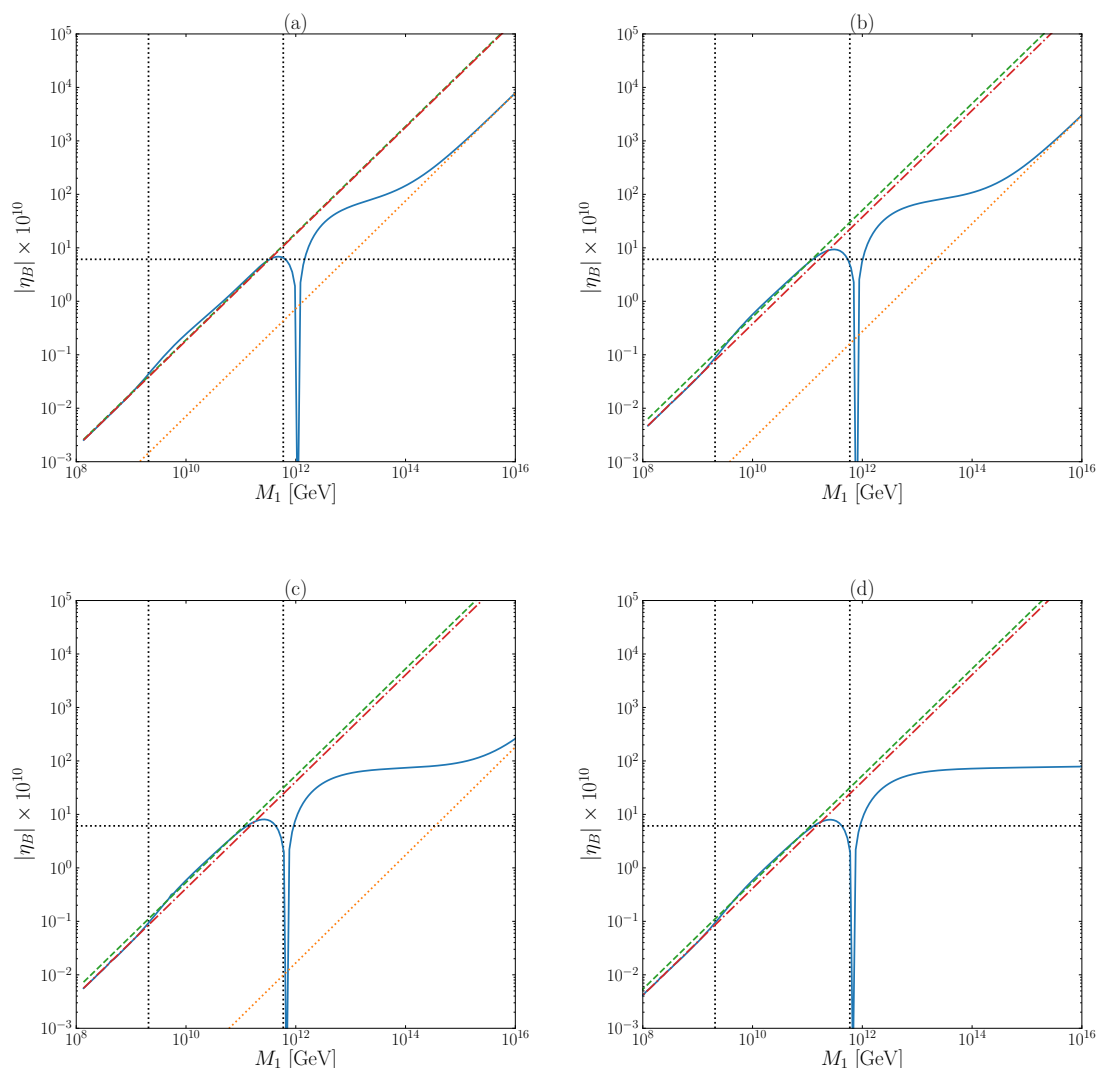in order to gain an analytical understanding of the numerical solutions.

Figure 14. The magnitude of the baryon asymmetry as a function of the heavy Majorana neutrino masses (assuming the modified Casas-Ibarra parametrisation) at a specific point in parameter space. The dotted orange line corresponds to solutions of the single-flavour Boltzmann equations, the dashed green line to those of the two-flavour Boltzmann equation, the red dot-dashed line to those of the three-flavour Boltzmann equations and the solid blue line to solutions of the density matrix equations. The horizontal black dotted line is the observed value of $\eta_{B_{\mathrm{CMB}}}$ and the vertical dotted lines to the values of the muon and tau thermal widths. We vary y_3 such that in (a) $y_3 = 30°$, in (b) $y_3 = 5°$, in (c) $y_3 = 0.3°$ and in (d) $y_3 = 0°$. As y_3 is the only complex parameter of the R-matrix for this parameter point, then plot (d) corresponds to the case of purely low-energy CP violation. As the CP violation becomes solely low energy (going from (a) to (d)), then the transition of the density matrix equations to the single-flavour regime becomes longer. This culminates in an infinite transition width in plot (d) — a plateau in the baryon asymmetry for high-scale leptogenesis. The dip in all of the blue lines occurs as a consequence of the change in sign of the produced asymmetry.
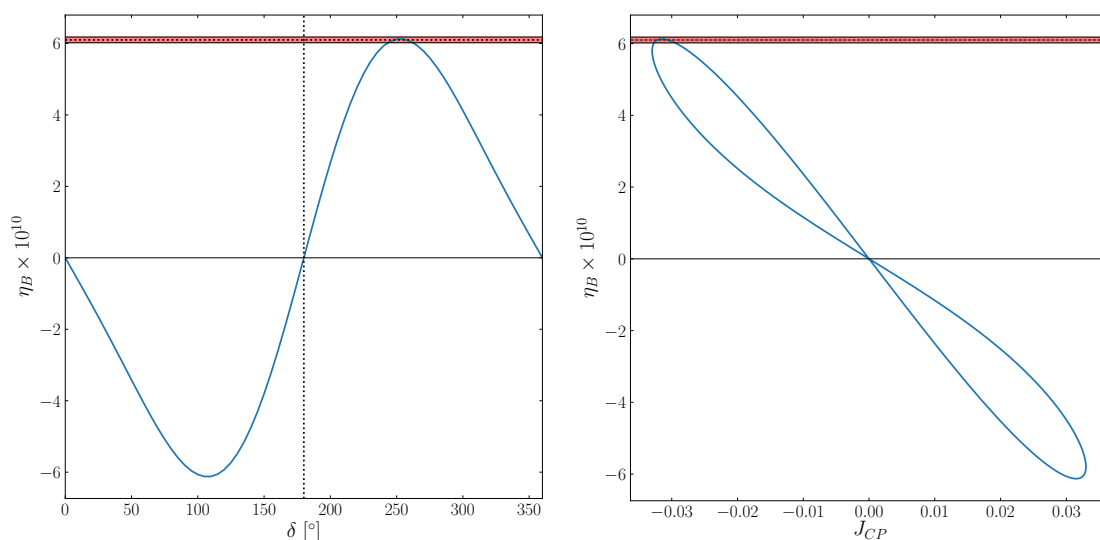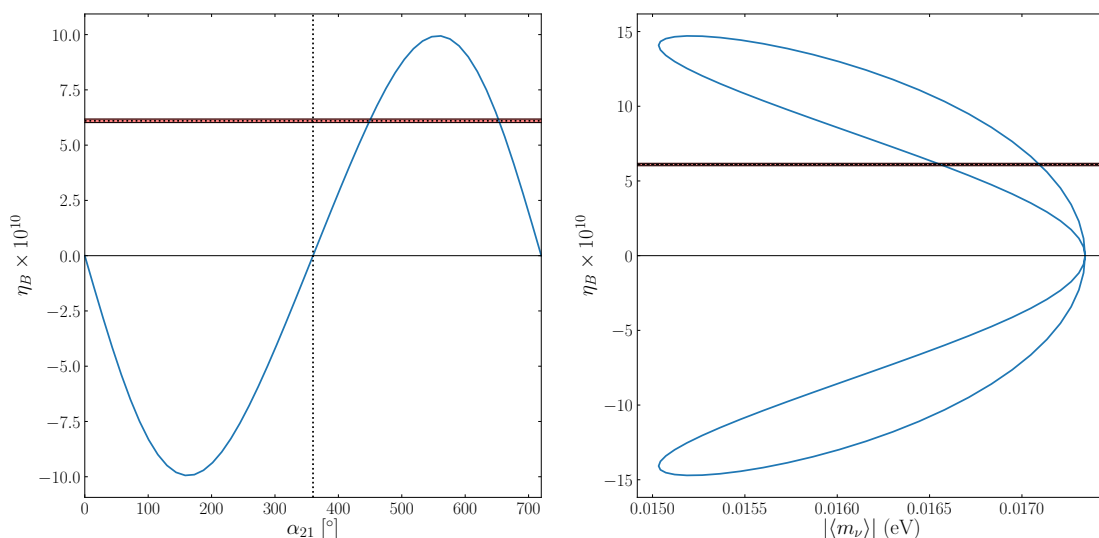
Figure 15. Leptogenesis at high scales ($M_1 = 3.16 \times 10^{13}$ GeV) with CP violation provided solely by δ, with $\alpha_{21} = 0°$ and $\alpha_{31} = 0°$. The red band indicates the 1σ observed values for η_B with the best-fit value indicated by the horizontal black dotted lines. Left: the baryon asymmetry as a function of δ with exact CP-invariance exists for $\delta = 0°$ and $180°$ (vertical black dotted lines). In order to make the maximum value touch on the observed baryon asymmetry, an amount of fine-tuning $\mathcal{F} = 105$ is needed. Right: the corresponding variation of η_B against $J_{\rm CP}$ parametrically plotted with δ. See the text for further details.

Figure 16. Leptogenesis at high scales ($M_1 = 3.16 \times 10^{13}$ GeV) when CP violation is provided solely by α_{21}, with $\delta = 0°$, $\alpha_{31} = 0°$. The red bands indicate the 1σ observed values for η_B with the best-fit value indicated by the horizontal black dotted lines. Left: the baryon asymmetry as a function of α_{21} with exact CP-invariance at $\alpha_{21} = 0°$ and $360°$ (vertical black dotted lines). Right: the variation of η_B against $|\langle m_\nu \rangle|$ parametrically plotted as a function of α_{21}. Successful leptogenesis occurs for $\alpha_{21} \approx 449°$ and $\alpha_{21} \approx 653°$ for which $|\langle m_\nu \rangle| = 0.0171$ eV and $|\langle m_\nu \rangle| = 0.0166$ eV respectively. See text for further details.

As in the analysis of section 4.1, we investigate the cases where CP violation comes from precisely one of δ, α_{21} or α_{31}. Unlike the fine-tuned scenario previously considered, $P_{\tau\tau}^{0(1)}$ and consequently ΔF are approximately constant with the PMNS phases as would be expected from our discussion of the fine-tuned solutions in section 4.2.4. Hence the phase-dependence of the η_B can be understood by reference to $\epsilon_{\tau\tau}^{(1)}$ alone. This may also be understood by reference to the Yukawa couplings when CP violation comes only from δ, α_{21} or α_{31} respectively:

$$
\begin{aligned}
Y_{\tau 1} &= -0.0476 - 0.000364 e^{i\delta}, \\
Y_{\tau 1} &= -0.0541 + 0.00614 e^{i\frac{\alpha_{21}}{2}}, \\
Y_{\tau 1} &= 0.00972 - 0.0576 e^{i\frac{\alpha_{31}}{2}}.
\end{aligned}
\tag{5.12}
$$

The difference in scale of the two terms means that the cancellation is never strong for any value of the phase and so the peaks in ΔF are not large. In this high scale case, ΔF is approximately constant and thus the plots of η_B exhibit a nearly pure sinusoidal variation given by the CP-asymmetries below.

5.3.1 Dirac phase CP violation

In this case, with a real R, we have $\alpha_{21} = \alpha_{31} = 0°$ such that δ is the sole provider of all CP violation. The asymmetry is given by

$$
\epsilon_{\tau\tau}^{(1)} = -1.25 \times 10^{-6} \sin\delta,
\tag{5.13}
$$

in this scenario. Thus we obtain a sinusoidal dependence with $\eta_B = 0$ when $\delta = 0°$ or $180°$. Fixing all other parameters at their benchmark value with $y_1 = y_2 = y_3 = 0$, no value of δ can produce the observed baryon asymmetry of the Universe. Unlike in the case of intermediate scale leptogenesis, a small scaling of the heavy Majorana neutrino masses will not much increase the value of η_B because of the plateau of figure 14. At the best-fit point of table 5, with $\alpha_{21} = \alpha_{31} = 0°$, allowing CP violation only from δ, the largest η_B achieved is a factor ~ 9 smaller than the observed value. This is large enough that even enormously larger scales of the heavy masses cannot make δ-only leptogenesis a viable option.

An alternative for producing the observed baryon asymmetry of the Universe with CP violation only from δ is to work with an R-matrix containing both zero and purely imaginary components which are CP-conserving and may potentially be large in magnitude. If for example, we choose $x_i = 0°$ such that all w_i are either purely imaginary or zero, and take $y_2 = 0°$ also, then by setting $\alpha_{21} = 180°$ and $\alpha_{31} = 0°$, all CP violation will be due to δ. Varying y_1 and y_2 together in this setup, we find that $y_1 = y_2 = 169°$ is the smallest value for which the observed baryon asymmetry of the Universe is produced. With all other parameters equal to the values in table 5, this corresponds to $\mathcal{F} = 105$. Hence a noticeable degree of fine-tuning is required even at high scales to make δ the sole contributor to CP violation with viable leptogenesis. In figure 15, we plot the variation of η_B with pure δ CP violation for this fine-tuned scenario in the left plot, and on the right we parametrically plot η_B against J_{CP} as a function of δ.

5.3.2 *CP* violation from the Majorana phase α_{21}

Similarly, when $\delta = \alpha_{31} = 0°$, the *CP*-asymmetry is

$$\epsilon_{\tau\tau}^{(1)} = 1.98 \times 10^{-5} \sin\frac{\alpha_{21}}{2}. \tag{5.14}$$

It follows from the preceding expression for $\epsilon_{\tau\tau}^{(1)}$ that at the *CP*-conserving values of $\alpha_{21} = 180°, 540°$ we have $\epsilon_{\tau\tau}^{(1)} \neq 0$. This corresponds to the case of *CP*-conserving *R*-matrix ($y_i = 0$), *CP*-conserving PMNS matrix, but *CP*-violating interplay between the *R* and PMNS matrix elements in leptogenesis [25].

The corresponding η_B, plotted in the left plot of figure 16 is thus a factor of $\mathcal{O}(10)$ higher and of opposite sign than in the previous case without fine-tuning. Thus, we obtain the observed baryon asymmetry of the Universe (or higher) for values of α_{21} between about $450°$ and $650°$. In the right plot of figure 16 is η_B for the same scenario parametrically plotted against the effective neutrino mass with parameter α_{21}.

5.3.3 *CP* violation from the Majorana phase α_{31}

Finally, we turn to the scenario in which *CP* violation is provided entirely by α_{31}, plotted on the left in of figure 17 for which

$$\epsilon_{\tau\tau}^{(1)} = -3.22 \times 10^{-5} \sin\frac{\alpha_{31}}{2}. \tag{5.15}$$

Similarly to the case discussed in the preceding subsection, we see that $\epsilon_{\tau\tau}^{(1)} \neq 0$ at the *CP*-conserving values of $\alpha_{31} = 180°, 540°$. This again corresponds to the case of *CP* violation in leptogenesis due to the interplay of the *CP*-conserving *R*-matrix ($y_i = 0$) and *CP*-conserving PMNS matrix [25].

Compared with the previous scenario, there is a sign flip and an enhancement by a factor ~ 1.6 of the resulting baryon asymmetry of the Universe. Thus, the observed BAU is achieved and exceeded for smaller values of α_{31}, between about $50°$ and $300°$. On the right of figure 17, we display a parametric plot for the same scenario with η_B against the effective neutrino Majorana mass with the parameter α_{31}.

6 Conclusions

In this paper we have investigated the connection between leptogenesis and low energy leptonic *CP* violation over a large range of scales $\left(10^6 < M_1 \,(\text{GeV}) < 10^{13}\right)$. We summarise our main findings below:

- Firstly, we revisited the question of the possibility of successful thermal leptogenesis at scales $10^9 < M_1 \,(\text{GeV}) < 10^{12}$. At such scales, tau-Yukawa interactions are in equilibrium, such that there are sufficiently frequent interactions between the leptons and the early Universe plasma causing decoherence between the tau flavour from the other flavour components. We show that successful leptogenesis is indeed possible in this range of scales in the case that the PMNS phases provide all of the *CP* violation in the model. By performing parameter explorations at $M_1 = 10^9 \,\text{GeV}$ and
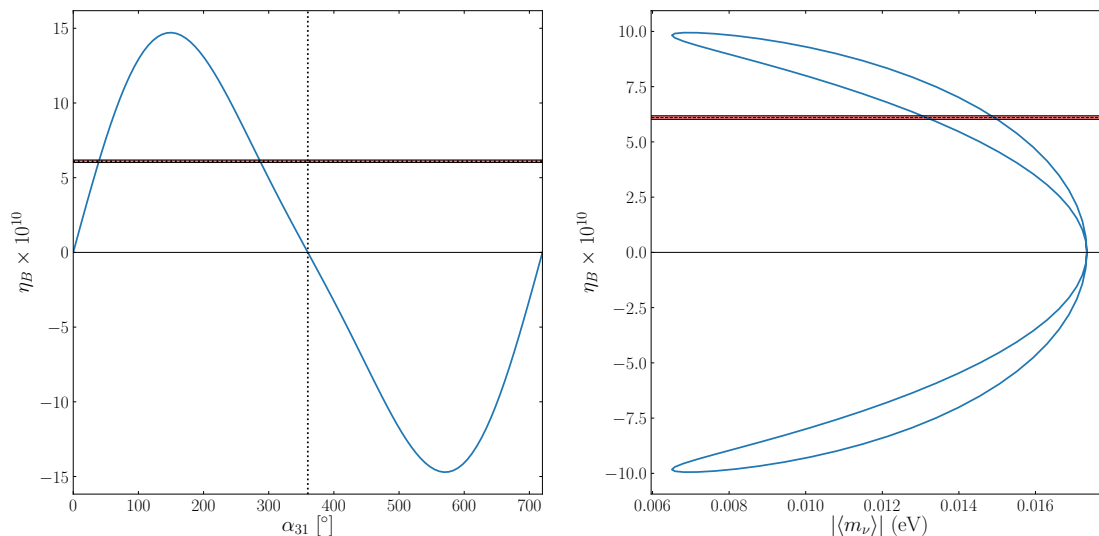
Figure 17. High-scale leptogenesis ($M_1 = 3.16 \times 10^{13}$ GeV) with CP violation is provided solely by α_{31}, with $\delta = 0°$, $\alpha_{21} = 0°$. The red bands indicate the 1σ observed values for η_B with the best-fit value indicated by the horizontal black dotted lines. Left: the baryon asymmetry as a function of α_{31}, with exact CP-invariance when $\alpha_{31} = 0°$ and $360°$ (vertical black dotted lines). Right: the parametric plot of η_B against the effective neutrino Majorana mass $|\langle m_\nu \rangle|$ as α_{31} is varied. At the values $\alpha_{31} = 17°, 43°$, η_B takes on its observed values corresponding to $|\langle m_\nu \rangle| = 0.0131$ eV, 0.0149 eV respectively. See the text for further details.

$M_1 = 10^{10}$ GeV, we found that some degree of fine-tuning, $\mathcal{F} \sim 10$, is required for these particular mass scales (with the degree of fine-tuning diminishing as one goes to higher values of M_1).

- By demanding pure Dirac phase or pure Majorana phase CP violation, we found that each phase alone can produce the correct CP-asymmetry, with the cases of Majorana phases requiring, in general, a somewhat lower value of M_1 than those required for the Dirac phase.

- If leptogenesis takes place at scales $M_1 \ll 10^9$ GeV, then all three of the leptonic flavour components involved in leptogenesis will decohere. For masses in this range ($M_1 \sim 10^6$ GeV and $M_1 \sim 10^8$ GeV), we determined the regions of parameter space in which low energy leptonic CP violation, provided by either the Dirac or the Majorana phases individually, leads to successful intermediate scale leptogenesis. At these scales a large amount of fine-tuning ($\mathcal{F} \sim \mathcal{O}(100)$) is required between the tree-level and one-loop neutrino masses. We restricted ourselves to fine-tuning such that $\mathcal{F} < 1000$ and in doing so have found an approximate lower bound of $M_1 \approx 3 \times 10^6$ GeV (consistent with the conclusions of [78]).

- We studied the possibility of pure Dirac phase CP violation and showed that for $\mathcal{F} < 1000$, $M_1 \gtrsim 8 \times 10^6$ GeV in order to produce the observed baryon asymmetry. Similarly for the purely Majorana phase CP violation and again $\mathcal{F} < 1000$, for α_{21}, we obtain a bound $M_1 \approx 4.5 \times 10^6$ GeV whereas for α_{31} we obtained $M_1 \approx 3 \times 10^6$ GeV.

Observables depending on the Dirac and Majorana phases, for example $J_{\rm CP}$ or $\langle m_\nu \rangle$, may be well within experimental bounds in the same parts of parameter space in which leptogenesis is successful. The Dirac phase δ is only very weakly constrained, with the tightest constraint being $\delta \in [16, 263]^\circ$, for 1σ agreement with the observed BAU, which comes from assuming normal ordering and $M_1 = 1.29 \times 10^8$ GeV.

- If leptogenesis takes place at high scales, with $M_1 \gg 10^{12}$ GeV, interactions between the leptons and the early Universe plasma only very weakly decohere the tau flavour from the other flavour components. Normally, this leads to the conclusion that the single flavour Boltzmann equations are an appropriate description of the process. However, we have demonstrated that, if CP violation arises only in the low energy leptonic sector, the effects of decoherence cannot be neglected. Therefore, one should not ignore the phenomenology of high-scale leptogenesis with purely low-energy CP violation.

- We explored the parameter space at $M_1 \sim 10^{13}$ GeV, finding regions in which thermal leptogenesis is a viable explanation of the BAU. We found that the strongest constraint on δ is for normal ordering, for which we require $\delta \in [240, 331]^\circ$ to produce a baryon asymmetry within 1σ of the observed value. With only Dirac phase CP violation, we have concluded that it is not possible produce the observed baryon asymmetry of the Universe unless one introduces significant fine-tuning ($\mathcal{F} \sim 100$) in the light neutrino masses. We argued that there is no scale of the heavy Majorana neutrino masses beyond $M_1 \gg 10^{12}$ GeV for which Dirac phase leptogenesis may be made to work without this fine-tuning. However, with pure Majorana phase violation, we found that successful leptogenesis is possible with essentially no fine-tuning.

The results of this article underscore the significance of understanding leptonic CP violation through experimental searches for Dirac and/or Majorana leptonic CP violation. We have departed from previous literature by concluding that low energy leptonic CP-violating phases may always be relevant to the production of the baryon asymmetry in the leptogenesis scenario. It has commonly been thought that their relevance was limited to the window of masses $10^9 \lesssim M_1\,({\rm GeV}) \lesssim 10^{12}$. However, we have shown this window to be significantly wider: Dirac and Majorana phases may be crucial to leptogenesis even at scales as low as $M_1 \sim 10^6$ GeV, or as high as $M_1 \gg 10^{12}$ GeV.

Acknowledgments

A   Classes of CP-Conserving R-matrix

With the parameters x_2, y_1 and y_3 left arbitrary, there are 16 possible R-matrices which lead to the fine-tuned light neutrino masses required for successful leptogenesis (eq. (2.27)). For any of these matrices, the absolute values of the elements $|R_{ij}|$ are equal, with the elements themselves differing only by factors ± 1 or $\pm i$. When there is an exact CP-symmetry, then each R-matrix satisfies the condition in eq. (2.16). This allows for a scheme of classification according the phases ρ^ν, ρ^N they correspond to. In this section we present a single example of a matrix for each class:[14] $\rho^\nu = \pm(-1, +1, +1)^T$, $\rho^N = \pm(+1, +1, -1)^T$ and $x_1 = 90°$ and $x_3 = 90°$:

$$R \approx \begin{pmatrix} -\frac{i}{2}e^{y_3}\cos x_2 & \frac{1}{2}e^{y_3}\cos x_2 & \sin x_2 \\ \frac{i}{4}e^{y_1+y_3}(\sin x_2 + 1) & -\frac{1}{4}e^{y_1+y_3}(\sin x_2 + 1) & \frac{1}{2}e^{y_1}\cos x_2 \\ \frac{1}{4}e^{y_1+y_3}(\sin x_2 + 1) & \frac{i}{4}e^{y_1+y_3}(\sin x_2 + 1) & -\frac{i}{2}e^{y_1}\cos x_2 \end{pmatrix},$$

in which the second form results from the neglect of terms involving factors e^{-y_1} and e^{-y_3}. $\rho^\nu = \pm(+1, -1, +1)^T$, $\rho^N = \pm(+1, -1, +1)^T$ and $x_1 = 0°$ and $x_3 = 0°$:

$$R \approx \begin{pmatrix} \frac{1}{2}e^{y_3}\cos x_2 & \frac{i}{2}e^{y_3}\cos x_2 & \sin x_2 \\ -\frac{i}{4}e^{y_1+y_3}(\sin x_2 + 1) & \frac{1}{4}e^{y_1+y_3}(\sin x_2 + 1) & \frac{i}{2}e^{y_1}\cos x_2 \\ -\frac{1}{4}e^{y_1+y_3}(\sin x_2 + 1) & -\frac{i}{4}e^{y_1+y_3}(\sin x_2 + 1) & \frac{1}{2}e^{y_1}\cos x_2 \end{pmatrix},$$

$\rho^\nu = \pm(+1, -1, +1)^T$, $\rho^N = \pm(+1, +1, -1)^T$ and $x_1 = 90°$ and $x_3 = 0°$:

$$R \approx \begin{pmatrix} \frac{1}{2}e^{y_3}\cos x_2 & \frac{i}{2}e^{y_3}\cos x_2 & \sin x_2 \\ -\frac{1}{4}e^{y_1+y_3}(\sin x_2 + 1) & -\frac{i}{4}e^{y_1+y_3}(\sin x_2 + 1) & \frac{1}{2}e^{y_1}\cos x_2 \\ \frac{i}{4}e^{y_1+y_3}(\sin x_2 + 1) & -\frac{1}{4}e^{y_1+y_3}(\sin x_2 + 1) & -\frac{i}{2}e^{y_1}\cos x_2 \end{pmatrix},$$

$\rho^\nu = \pm(-1, +1, +1)^T$, $\rho^N = \pm(+1, -1, +1)^T$ and $x_1 = 90°$ and $x_3 = 0°$:

$$R \approx \begin{pmatrix} -\frac{i}{2}e^{y_3}\cos x_2 & \frac{1}{2}e^{y_3}\cos x_2 & \sin x_2 \\ -\frac{1}{4}e^{y_1+y_3}(\sin x_2 + 1) & -\frac{i}{4}e^{y_1+y_3}(\sin x_2 + 1) & \frac{i}{2}e^{y_1}\cos x_2 \\ \frac{i}{4}e^{y_1+y_3}(\sin x_2 + 1) & -\frac{1}{4}e^{y_1+y_3}(\sin x_2 + 1) & \frac{1}{2}e^{y_1}\cos x_2 \end{pmatrix}.$$

[14]Here we neglect terms involving factors e^{-y_1} or e^{-y_3} such that, as given, these matrices are not strictly orthogonal.
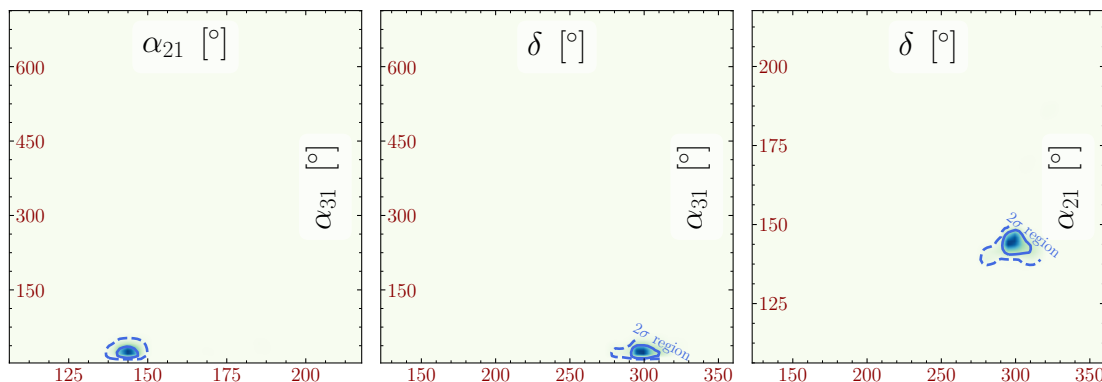
Figure 18. The two-dimensional projections for intermediate scale leptogenesis with $M_1 = 3.16 \times 10^6$ GeV and $m_1 = 0.05$ eV with CP violation provided only by the phases of the PMNS matrix. Solid lines correspond to 68% confidence level and dashed to 95% confidence level in agreement with the observed value $\eta_{B_{\mathrm{CMB}}}$. This plot was created using SuperPlot [88].

B Further results

In figure 18 we demonstrate the possibility of fine-tuned leptogenesis in the case of normal ordering with $M_1 = 3.16 \times 10^6$ GeV and $m_1 = 0.05$ eV. This is a variant of the case considered in the main body for which the light neutrino masses are significantly reduced below all present cosmological or current generation direct bounds. We note that lowering the light neutrino masses in this way severely constrains the viable parameter space over that in figure 8 such that $\delta \approx 296°$, $\alpha_{21} \approx 143°$ and $\alpha_{31} \approx 14°$. Typical fine-tuning in the viable regions is $\mathcal{F} \approx 450$.

In the cases of $m_1 = 0$ and $m_1 = 10^{-3}$ eV with $M_1 = 10^8$ GeV, $M_2 = 3M_1$ and $M_3 = 3M_2$ we did not find a region in the relevant parameter space in which one could have successful leptogenesis.

In figure 19 we present results for $M_1 = 10^9$ GeV. We find that a fine-tuning of the light neutrino masses $\mathcal{F} \approx 14$ at the best-fit points. In the normal ordered case, we find that the observed baryon asymmetry may be obtained to within 1σ (2σ) with δ between $[0, 360]°$ ($[0, 360]°$). While for inverted ordering, the 1σ (2σ) range is $[25, 360]°$ ($[0, 360]°$). This is significantly higher than the case for which $M_1 = 10^{10}$ GeV where the fine-tuning is considerably less at $\mathcal{F} \approx 0.23$. In the normal ordered case, we find that the observed baryon asymmetry may be obtained to within 1σ (2σ) with δ between $[95, 265]°$ ($[52, 282]°$). For inverted ordering, the 1σ (2σ) range is $[60, 338]°$ ($[8, 360]°$).

C Single flavour boltzmann equations from density matrix equations

In this appendix we find the conditions under which the density matrix equations (eq. (2.49)) approximate to the single flavour Boltzmann equations. We begin by analysing the criteria under which the single flavour Boltzmann equation

$$\frac{dn_{B-L}}{dz} = \mathrm{Tr}\,\epsilon^{(1)} D_1 (n_{N_1} - n_N^{\mathrm{eq}}) - W_1 n_{B-L}, \tag{C.1}$$
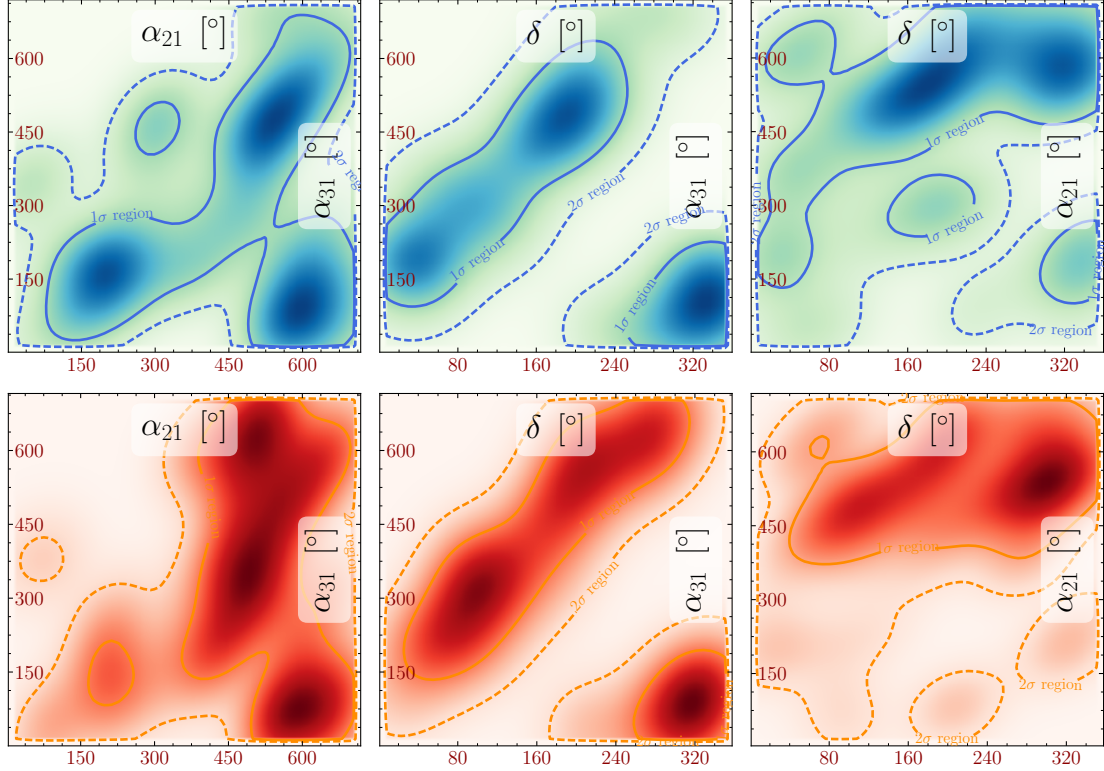
Figure 19. The two-dimensional projections for leptogenesis with $M_1 = 1.00 \times 10^9 \, \text{GeV}$ with CP violation provided only by the phases of the PMNS matrix. The normal ordered case is coloured blue/green and inverted ordering orange/red and contours correspond to 68% and 95% confidence levels. This plot was created using SUPERPLOT [88].

emerges as an approximation from the density matrix equations, which, written in the $(\tau^\perp, \tau)$-basis are

$$\frac{dn_{N_1}}{dz} = -D_1 \left(n_{N_1} - n_{N_1}^{\text{eq}} \right)$$

$$\frac{dn_{\tau^\perp \tau^\perp}}{dz} = \epsilon_{\tau^\perp \tau^\perp}^{(1)} D_1 \left(n_{N_1} - n_{N_1}^{\text{eq}} \right) - \frac{1}{2} W_1 \left(2|C_{1\tau^\perp}|^2 n_{\tau^\perp \tau^\perp} + C_{1\tau}^* C_{1\tau^\perp} n_{\tau\tau^\perp} + C_{1\tau} C_{1\tau^\perp}^* n_{\tau^\perp \tau} \right)$$

$$\frac{dn_{\tau\tau}}{dz} = \epsilon_{\tau\tau}^{(1)} D_1 \left(n_{N_1} - n_{N_1}^{\text{eq}} \right) - \frac{1}{2} W_1 \left(2|C_{1\tau}|^2 n_{\tau\tau} + C_{1\tau}^* C_{1\tau^\perp} n_{\tau\tau^\perp} + C_{1\tau} C_{1\tau^\perp}^* n_{\tau^\perp \tau} \right)$$

$$\frac{dn_{\tau^\perp \tau}}{dz} = \epsilon_{\tau^\perp \tau}^{(1)} D_1 \left(n_{N_1} - n_{N_1}^{\text{eq}} \right) - \frac{1}{2} W_1 \left(n_{\tau^\perp \tau} + C_{1\tau}^* C_{1\tau^\perp} \left(n_{\tau^\perp \tau^\perp} + n_{\tau\tau} \right) \right) - \frac{\text{Im} \left(\Lambda_\tau \right)}{Hz} n_{\tau^\perp \tau}.$$
(C.2)

As $n_{B-L} = n_{\tau\tau} + n_{\tau^\perp \tau^\perp}$, we find an equation for the evolution of n_{B-L} by adding the second and third equations together, obtaining

$$\frac{dn_{B-L}}{dz} = D_1 \left(n_{N_1} - n_{N_1}^{\text{eq}} \right) \text{Tr} \, \epsilon^{(1)} - W_1 \left(|C_{1\tau}|^2 n_{\tau\tau} + |C_{1\tau^\perp}|^2 n_{\tau^\perp \tau^\perp} + 2\Re[C_{1\tau^\perp} C_{1\tau}^* n_{\tau\tau^\perp}] \right).$$
(C.3)

If this were to reproduce the single flavour limit, then we should find that the coefficient of W_1:

$$|C_{1\tau}|^2 n_{\tau\tau} + |C_{1\tau^\perp}|^2 n_{\tau^\perp \tau^\perp} + 2\Re[C_{1\tau^\perp} C_{1\tau}^* n_{\tau\tau^\perp}],$$
(C.4)

is equal to n_{B-L} in the limit that $\mathrm{Im}(\Lambda_\tau)/Hz$ is small. Recalling that $|C_{1\tau^\perp}|^2 + |C_{1\tau}|^2 = 1$, then one should expect, that in the limit of small thermal widths,

$$2\Re[C_{1\tau^\perp}C_{1\tau}^* n_{\tau\tau^\perp}] = |C_{1\tau^\perp}|^2 n_{\tau\tau} + |C_{1\tau}|^2 n_{\tau^\perp\tau^\perp}. \tag{C.5}$$

In order to demonstrate this equality, first we show that the z-derivative of $2\Re[C_{1\tau^\perp}C_{1\tau}^* n_{\tau\tau^\perp}]$ equals the z-derivative of $|C_{1\tau^\perp}|^2 n_{\tau\tau} + |C_{1\tau}|^2 n_{\tau^\perp\tau^\perp}$ meaning that the quantities themselves may differ only by a constant. Then we note that, since at $z = z_0$ the quantities are equal, then they must be equal for all z.

By multiplication of the relevant equations in eq. (C.2), we obtain the z-evolution of $|C_{1\tau^\perp}|^2 n_{\tau\tau} + |C_{1\tau}|^2 n_{\tau^\perp\tau^\perp}$:

$$|C_{1\tau^\perp}|^2 \frac{dn_{\tau\tau}}{dz} + |C_{1\tau}|^2 \frac{dn_{\tau^\perp\tau^\perp}}{dz} = (|C_{1\tau^\perp}|^2 \epsilon_{\tau\tau}^{(1)} + |C_{1\tau}|^2 \epsilon_{\tau^\perp\tau^\perp}^{(1)}) D_1(n_{N_1} - n_{N_1}^{\mathrm{eq}})$$
$$- W_1(\Re[C_{1\tau^\perp}C_{1\tau}^* n_{\tau\tau^\perp}] + |C_{1\tau^\perp}|^2|C_{1\tau}|^2(n_{\tau\tau} + n_{\tau^\perp\tau^\perp})). \tag{C.6}$$

By similar means we obtain the z-evolution of $\Re[C_{1\tau^\perp}C_{1\tau}^* n_{\tau\tau^\perp}]$:

$$\Re\left[C_{1\tau^\perp}C_{1\tau}^* \frac{dn_{\tau\tau^\perp}}{dz}\right] = \Re\left[C_{1\tau^\perp}C_{1\tau}^* \epsilon_{\tau\tau^\perp}^{(1)}\right] D_1(n_{N_1} - n_{N_1}^{\mathrm{eq}})$$
$$- \frac{1}{2}W_1(\Re[C_{1\tau^\perp}C_{1\tau}^* n_{\tau\tau^\perp}] + |C_{1\tau^\perp}|^2|C_{1\tau}|^2(n_{\tau\tau} + n_{\tau^\perp\tau^\perp})) \tag{C.7}$$
$$- \Re[C_{1\tau^\perp}C_{1\tau}^* n_{\tau\tau^\perp}] \frac{\Im(\Lambda_\tau)}{Hz}.$$

Neglecting $\Im(\Lambda_\tau)/Hz$, as we expect this to be small in the single-flavour regime, then we need only show that

$$2\Re\left[C_{1\tau^\perp}C_{1\tau}^* \epsilon_{\tau\tau^\perp}^{(1)}\right] = |C_{1\tau^\perp}|^2 \epsilon_{\tau\tau}^{(1)} + |C_{1\tau}|^2 \epsilon_{\tau^\perp\tau^\perp}^{(1)}, \tag{C.8}$$

and then it is demonstrated that the coefficient of W_1 in eq. (C.3) is approximately equal to n_{B-L} and thus the single flavour equations are recovered.

The relation of eq. (C.8) can be put into a more suggestive form if we use $|C_{1\tau^\perp}|^2 = 1 - |C_{1\tau}|^2$ to re-express it thus

$$2\Re[C_{1\tau^\perp}C_{1\tau}^* \epsilon_{\tau\tau^\perp}^{(1)}] + |C_{1\tau^\perp}|^2 \epsilon_{1\tau^\perp}^{(1)} + |C_{1\tau}|^2 \epsilon_{1\tau}^{(1)} = \epsilon_{\tau\tau}^{(1)} + \epsilon_{\tau^\perp\tau^\perp}^{(1)}. \tag{C.9}$$

The right-hand side of this equation is merely the trace of the CP-asymmetry tensor $\mathrm{Tr}\,\epsilon^{(1)}$ in the $(\tau^\perp, \tau)$-basis. Thus, we suspect that the left-hand side is merely the trace expressed in an unfamiliar basis. This can be confirmed to be the case by construction of the unitary matrix

$$S = \begin{pmatrix} C_{1\tau} & -C_{1\tau^\perp}^* \\ C_{1\tau^\perp} & C_{1\tau}^* \end{pmatrix}, \tag{C.10}$$

then, by explicit calculation it can be seen that the left-hand side is the result of summing the diagonals (evaluating the trace in a particular basis) of

$$S^\dagger \epsilon^{(1)} S. \tag{C.11}$$

Thus, we may conclude that, if we set $\Im(\Lambda_\tau) = 0$, we are left with

$$2\Re\left[C_{1\tau\perp}C^*_{1\tau}\frac{dn_{\tau\tau\perp}}{dz}\right] = |C_{1\tau\perp}|^2\frac{dn_{\tau\tau}}{dz} + |C_{1\tau}|^2\frac{dn_{\tau\perp\tau\perp}}{dz}, \tag{C.12}$$

and so

$$\frac{d}{dz}(|C_{1\tau}|^2 n_{\tau\tau} + |C_{1\tau\perp}|^2 n_{\tau\perp\tau\perp} + 2\Re[C_{1\tau\perp}C^*_{1\tau}n_{\tau\tau\perp}]) = \frac{dn_{B-L}}{dz}. \tag{C.13}$$

Since $n_{\alpha\beta} = 0$ at the initial z, then we may conclude that, if $\Im(\Lambda_\tau) = 0$, then

$$\frac{dn_{B-L}}{dz} = \operatorname{Tr}\epsilon^{(1)}D(n_{N_1} - n_{N_1}^{\mathrm{eq}}) - W_1 n_{B-L}, \tag{C.14}$$

which is the single-flavour limit.

If we don't set $\Im(\Lambda_\tau) = 0$, then we have

$$\frac{d}{dz}(|C_{1\tau}|^2 n_{\tau\tau} + |C_{1\tau\perp}|^2 n_{\tau\perp\tau\perp} + 2\Re[C_{1\tau\perp}C^*_{1\tau}n_{\tau\tau\perp}]) = \frac{dn_{B-L}}{dz} - 2\Re\left[C_{1\tau\perp}C^*_{1\tau}\frac{\Im(\Lambda_\tau)}{Hz}n_{\tau\tau\perp}\right], \tag{C.15}$$

which suggests that we should write the integro-differential equation

$$\frac{dn_{B-L}}{dz} = \operatorname{Tr}\epsilon^{(1)}D_1(n_{N_1} - n_{N_1}^{\mathrm{eq}}) - W_1 n_{B-L} + 2W_1\int_{z_0}^z dz'\Re\left[C_{1\tau\perp}C^*_{1\tau}\frac{\Im(\Lambda_\tau)}{Hz'}n_{\tau\tau\perp}(z')\right]. \tag{C.16}$$

We define

$$\lambda(z) \equiv 2\int_{z_0}^z dz'\Re\left[C_{1\tau\perp}C^*_{1\tau}\frac{\Im(\Lambda_\tau)}{Hz'}n_{\tau\tau\perp}(z')\right], \tag{C.17}$$

for brevity, then using the integrating factor method, arrive at a solution

$$\begin{aligned}
n_{B-L}(z_f) &= e^{-\int_{z_0}^{z_f} W_1(z)dz}\int_{z_0}^{z_f} e^{\int_{z_0}^{z'} W_1(z'')dz''} \\
&\qquad\times\left(\operatorname{Tr}\epsilon^{(1)}D_1(z')(n_{N_1}(z') - n_{N_1}^{\mathrm{eq}}(z')) + W_1(z')\lambda(z')\right)dz' \\
&= \int_{z_0}^{z_f} e^{-\int_{z'}^{z_f} W(z'')dz''}\left(\operatorname{Tr}\epsilon^{(1)}D_1(z')(n_{N_1}(z') - n_{N_1}^{\mathrm{eq}}(z')) + W_1(z')\lambda(z')\right)dz'.
\end{aligned}$$

For large M_1, the thermal width is very small and so the term in λ is usually neglected in comparison with the first.

D Robustness of the high-scale plateau

In the transition region, the approximation that left-handed τ leptons are produced and destroyed at the same rate by flavour effects is somewhat inaccurate. In fact we should consider a slightly more accurate version of the density matrix equations in which the asymmetry density of right-handed τ leptons, $n_{\tau R}$ is computed. Then, the density matrix

equations are

$$\frac{dn_{N_1}}{dz} = -D_1\left(n_{N_1} - n_{N_1}^{\text{eq}}\right)$$

$$\frac{dn_{\tau^\perp\tau^\perp}}{dz} = \epsilon^{(1)}_{\tau^\perp\tau^\perp}D_1\left(n_{N_1} - n_{N_1}^{\text{eq}}\right) - \frac{1}{2}W_1\left(2|C_{1\tau^\perp}|^2 n_{\tau^\perp\tau^\perp} + C^*_{1\tau}C_{1\tau^\perp}n_{\tau\tau^\perp} + C_{1\tau}C^*_{1\tau^\perp}n_{\tau^\perp\tau}\right)$$

$$\frac{dn_{\tau\tau}}{dz} = \epsilon^{(1)}_{\tau\tau}D_1\left(n_{N_1} - n_{N_1}^{\text{eq}}\right) - \frac{1}{2}W_1\left(2|C_{1\tau}|^2 n_{\tau\tau} + C^*_{1\tau}C_{1\tau^\perp}n_{\tau\tau^\perp} + C_{1\tau}C^*_{1\tau^\perp}n_{\tau^\perp\tau}\right)$$

$$\qquad - 2\frac{\Im(\Lambda_\tau)}{Hz}(n_{\tau\tau} - 2n_{\tau_R})$$

$$\frac{dn_{\tau^\perp\tau}}{dz} = \epsilon_{\tau^\perp\tau}D_1\left(n_{N_1} - n_{N_1}^{\text{eq}}\right) - \frac{1}{2}W_1\left(n_{\tau^\perp\tau} + C^*_{1\tau}C_{1\tau^\perp}\left(n_{\tau^\perp\tau^\perp} + n_{\tau\tau}\right)\right) - \frac{\text{Im}\left(\Lambda_\tau\right)}{Hz}n_{\tau^\perp\tau}$$

$$\frac{dn_{\tau_R}}{dz} = 2\frac{\Im(\Lambda_\tau)}{Hz}(n_{\tau\tau} - 2n_{\tau_R}).$$

$$\text{(D.1)}$$

The simpler set we previously considered result from the assumption that $\Im(\Lambda_\tau)/Hz$ is large enough to enforce $n_{\tau\tau} = 2n_{\tau_R}$. Clearly this is inaccurate for the situation under consideration where $M_1 \gg 10^{12}$ GeV. We should now append to $\lambda(z)$ an extra term such that

$$\lambda(z) \to \lambda'(z) = 2\int_{z_0}^z dz'\left(\Re\left[C_{1\tau^\perp}C^*_{1\tau}\frac{\Im(\Lambda_\tau)}{Hz'}n_{\tau\tau^\perp}(z')\right] - 2\frac{\Im(\Lambda_\tau)}{Hz'}(n_{\tau\tau}(z') - 2n_{\tau R}(z'))\right). \tag{D.2}$$

Now in this solution, there is a term in $n_{\tau\tau}\Im(\Lambda_\tau)/Hz$ which scales approximately as $xx^{-1} = x^0$ and a term $n_{\tau R}\Im(\Lambda_\tau)/Hz$ in which, it may be shown $n_{\tau R} \propto x$ and thus $\lambda'(z)$ exhibits a approximate invariance under a scaling x as does $\lambda(z)$.

It may be added that scattering effects can be incorporated by modifying the decay function $D_1(z) \to D_1'(z) = D_1(z) + S_1(z)$ and the washout $W_1(z) \to W_1'(z) = j(z)W_1(z)$ [11]. The new decay function $D_1'(z)$ which depends on a scattering part $S_1(z)$ is still multiplied by zero in the Tr $\epsilon = 0$ case and is thus unimportant. The new washout function is multiplied by $j(z)$ which depends on M_1 through $\log(M_1/m_H)$. Thus, the plateau demonstrated in figure 14 picks up some unimportant logarithmic dependence on M_1 in addition to the small variation when scattering is neglected. In the numerical calculations of section 5, the effects of scattering are included.

Open Access. This article is distributed under the terms of the Creative Commons Attribution License ([CC-BY 4.0](https://creativecommons.org/licenses/by/4.0)), which permits any use, distribution and reproduction in any medium, provided the original author(s) and source are credited.

References

[1] A.D. Sakharov, *Violation of CP Invariance, C asymmetry and baryon asymmetry of the universe*, *Pisma Zh. Eksp. Teor. Fiz.* **5** (1967) 32 [INSPIRE].

[2] SUPER-KAMIOKANDE collaboration, *Evidence for oscillation of atmospheric neutrinos*, *Phys. Rev. Lett.* **81** (1998) 1562 [hep-ex/9807003] [INSPIRE].

[3] V.A. Kuzmin, V.A. Rubakov and M.E. Shaposhnikov, *On the anomalous electroweak baryon number nonconservation in the early universe*, *Phys. Lett.* **B 155** (1985) 36.

[4] S.Yu. Khlebnikov and M.E. Shaposhnikov, *The statistical theory of anomalous fermion number nonconservation*, *Nucl. Phys.* **B 308** (1988) 885 [ɪɴSPIRE].

[5] P. Minkowski, $\mu \to e\gamma$ *at a rate of one out of* 10^9 *muon decays?*, *Phys. Lett.* **67B** (1977) 421 [ɪɴSPIRE].

[6] T. Yanagida, *Horizontal gauge symmetry and masses of neutrinos*, *Conf. Proc.* **C 7902131** (1979) 95 [ɪɴSPIRE].

[7] M. Gell-Mann, P. Ramond and R. Slansky, *Complex spinors and unified theories*, *Conf. Proc.* **C 790927** (1979) 315 [arXiv:1306.4669] [ɪɴSPIRE].

[8] R.N. Mohapatra and G. Senjanović, *Neutrino mass and spontaneous parity nonconservation*, *Phys. Rev. Lett.* **44** (1980) 912 [ɪɴSPIRE].

[9] M. Fukugita and T. Yanagida, *Baryogenesis without grand unification*, *Phys. Lett.* **B 174** (1986) 45 [ɪɴSPIRE].

[10] W. Buchmüller and M. Plümacher, *Baryon asymmetry and neutrino mixing*, *Phys. Lett.* **B 389** (1996) 73 [hep-ph/9608308] [ɪɴSPIRE].

[11] W. Buchmüller, P. Di Bari and M. Plümacher, *Leptogenesis for pedestrians*, *Annals Phys.* **315** (2005) 305 [hep-ph/0401240] [ɪɴSPIRE].

[12] W. Buchmüller, R.D. Peccei and T. Yanagida, *Leptogenesis as the origin of matter*, *Ann. Rev. Nucl. Part. Sci.* **55** (2005) 311 [hep-ph/0502169] [ɪɴSPIRE].

[13] A. Pilaftsis, *CP violation and baryogenesis due to heavy Majorana neutrinos*, *Phys. Rev.* **D 56** (1997) 5431 [hep-ph/9707235] [ɪɴSPIRE].

[14] PARTICLE DATA GROUP collaboration, *Review of particle physics*, *Phys. Rev.* **D 98** (2018) 030001 [ɪɴSPIRE].

[15] G.C. Branco, T. Morozumi, B.M. Nobre and M.N. Rebelo, *A bridge between CP-violation at low-energies and leptogenesis*, *Nucl. Phys.* **B 617** (2001) 475 [hep-ph/0107164] [ɪɴSPIRE].

[16] G.C. Branco et al., *Minimal scenarios for leptogenesis and CP-violation*, *Phys. Rev.* **D 67** (2003) 073025 [hep-ph/0211001] [ɪɴSPIRE].

[17] T. Endoh et al., *CP violation in neutrino oscillation and leptogenesis*, *Phys. Rev. Lett.* **89** (2002) 231601 [hep-ph/0209020] [ɪɴSPIRE].

[18] P.H. Frampton, S.L. Glashow and T. Yanagida, *Cosmological sign of neutrino CP-violation*, *Phys. Lett.* **B 548** (2002) 119 [hep-ph/0208157] [ɪɴSPIRE].

[19] Y. Shimizu, K. Takagi and M. Tanimoto, *Neutrino CP-violation and sign of baryon asymmetry in the minimal seesaw model*, *Phys. Lett.* **B 778** (2018) 6 [arXiv:1711.03863] [ɪɴSPIRE].

[20] E. Nardi, Y. Nir, J. Racker and E. Roulet, *On Higgs and sphaleron effects during the leptogenesis era*, *JHEP* **01** (2006) 068 [hep-ph/0512052] [ɪɴSPIRE].

[21] A. Abada et al., *Flavour matters in leptogenesis*, *JHEP* **09** (2006) 010 [hep-ph/0605281] [ɪɴSPIRE].

[22] A. Abada et al., *Flavor issues in leptogenesis*, *JCAP* **04** (2006) 004 [hep-ph/0601083] [ɪɴSPIRE].

[23] R. Barbieri, P. Creminelli, A. Strumia and N. Tetradis, *Baryogenesis through leptogenesis*, *Nucl. Phys.* **B 575** (2000) 61 [hep-ph/9911315] [ɪɴSPIRE].

[24] H.B. Nielsen and Y. Takanishi, *Baryogenesis via lepton number violation and family replicated gauge group*, *Nucl. Phys.* **B 636** (2002) 305 [hep-ph/0204027] [INSPIRE].

[25] S. Pascoli, S.T. Petcov and A. Riotto, *Connecting low energy leptonic CP-violation to leptogenesis*, *Phys. Rev.* **D 75** (2007) 083511 [hep-ph/0609125] [INSPIRE].

[26] S. Pascoli, S.T. Petcov and A. Riotto, *Leptogenesis and low energy CP-violation in neutrino physics*, *Nucl. Phys.* **B 774** (2007) 1 [hep-ph/0611338] [INSPIRE].

[27] S. Blanchet and P. Di Bari, *Flavor effects on leptogenesis predictions*, *JCAP* **03** (2007) 018 [hep-ph/0607330] [INSPIRE].

[28] G.C. Branco, R. Gonzalez Felipe and F.R. Joaquim, *A new bridge between leptonic CP-violation and leptogenesis*, *Phys. Lett.* **B 645** (2007) 432 [hep-ph/0609297] [INSPIRE].

[29] A. Anisimov, S. Blanchet and P. Di Bari, *Viability of Dirac phase leptogenesis*, *JCAP* **04** (2008) 033 [arXiv:0707.3024] [INSPIRE].

[30] E. Molinaro and S.T. Petcov, *The interplay between the 'low' and 'high' energy CP-violation in leptogenesis*, *Eur. Phys. J.* **C 61** (2009) 93 [arXiv:0803.4120] [INSPIRE].

[31] E. Molinaro and S.T. Petcov, *A case of subdominant/suppressed 'high energy' contribution to the baryon asymmetry of the universe in flavoured leptogenesis*, *Phys. Lett.* **B 671** (2009) 60 [arXiv:0808.3534] [INSPIRE].

[32] M.J. Dolan, T.P. Dutka and R.R. Volkas, *Dirac-phase thermal leptogenesis in the extended Type-I seesaw model*, *JCAP* **06** (2018) 012 [arXiv:1802.08373] [INSPIRE].

[33] C. Hagedorn et al., *CP violation in the lepton sector and implications for leptogenesis*, *Int. J. Mod. Phys.* **A 33** (2018) 1842006 [arXiv:1711.02866] [INSPIRE].

[34] G.C. Branco et al., *Another look at minimal lepton flavour violation, $l_i \to l_{j\gamma}$, leptogenesis and the ratio M_ν/Λ_{LFV}*, *JHEP* **09** (2007) 004 [hep-ph/0609067] [INSPIRE].

[35] L. Merlo and S. Rosauro-Alcaraz, *Predictive leptogenesis from minimal lepton flavour violation*, *JHEP* **07** (2018) 036 [arXiv:1801.03937] [INSPIRE].

[36] C.C. Nishi, B.L. Sánchez-Vega and G. Souza Silva, *$\mu\tau$ reflection symmetry with a high scale texture-zero*, *JHEP* **09** (2018) 042 [arXiv:1806.07412] [INSPIRE].

[37] A. Meroni, E. Molinaro and S.T. Petcov, *Revisiting leptogenesis in a SUSY SU(5) × T′ model of flavour*, *Phys. Lett.* **B 710** (2012) 435 [arXiv:1203.4435] [INSPIRE].

[38] R.N. Mohapatra and C.C. Nishi, *Implications of μ-τ flavored CP symmetry of leptons*, *JHEP* **08** (2015) 092 [arXiv:1506.06788] [INSPIRE].

[39] C. Hagedorn and E. Molinaro, *Flavor and CP symmetries for leptogenesis and $0\nu\beta\beta$ decay*, *Nucl. Phys.* **B 919** (2017) 404 [arXiv:1602.04206] [INSPIRE].

[40] P. Chen, G.-J. Ding and S.F. King, *Leptogenesis and residual CP symmetry*, *JHEP* **03** (2016) 206 [arXiv:1602.03873] [INSPIRE].

[41] C.-C. Li and G.-J. Ding, *Implications of residual CP symmetry for leptogenesis in a model with two right-handed neutrinos*, *Phys. Rev.* **D 96** (2017) 075005 [arXiv:1701.08508] [INSPIRE].

[42] L. Covi, J.E. Kim, B. Kyae and S. Nam, *Leptogenesis with high-scale electroweak symmetry breaking and an extended Higgs sector*, *Phys. Rev.* **D 94** (2016) 065004 [arXiv:1601.00411] [INSPIRE].

[43] S.M. Bilenky, J. Hosek and S.T. Petcov, *On oscillations of neutrinos with Dirac and Majorana masses*, *Phys. Lett.* **B 94** (1980) 495.

[44] I. Esteban et al., *Updated fit to three neutrino mixing: exploring the accelerator-reactor complementarity*, *JHEP* **01** (2017) 087 [`arXiv:1611.01514`] [InSPIRE].

[45] A. Pilaftsis, *Radiatively induced neutrino masses and large Higgs neutrino couplings in the standard model with Majorana fields*, *Z. Phys.* **C 55** (1992) 275 [`hep-ph/9901206`] [InSPIRE].

[46] D. Aristizabal Sierra and C.E. Yaguna, *On the importance of the 1-loop finite corrections to seesaw neutrino masses*, *JHEP* **08** (2011) 013 [`arXiv:1106.3587`] [InSPIRE].

[47] J. Lopez-Pavon, S. Pascoli and C.-f. Wong, *Can heavy neutrinos dominate neutrinoless double beta decay?*, *Phys. Rev.* **D 87** (2013) 093007 [`arXiv:1209.5342`] [InSPIRE].

[48] W. Grimus and L. Lavoura, *One-loop corrections to the seesaw mechanism in the multi-Higgs-doublet standard model*, *Phys. Lett.* **B 546** (2002) 86 [`hep-ph/0207229`] [InSPIRE].

[49] J.A. Casas and A. Ibarra, *Oscillating neutrinos and $\mu \to e$, γ*, *Nucl. Phys.* **B 618** (2001) 171 [`hep-ph/0103065`] [InSPIRE].

[50] J. Lopez-Pavon, E. Molinaro and S.T. Petcov, *Radiative corrections to light neutrino masses in low scale Type I seesaw scenarios and neutrinoless double beta decay*, *JHEP* **11** (2015) 030 [`arXiv:1506.05296`] [InSPIRE].

[51] S.M. Bilenky and S.T. Petcov, *Massive neutrinos and neutrino oscillations*, *Rev. Mod. Phys.* **59** (1987) 671 [*Erratum ibid.* **61** (1989) 169] [InSPIRE].

[52] T2K collaboration, *The T2K experiment*, *Nucl. Instrum. Meth.* **A 659** (2011) 106 [`arXiv:1106.1238`] [InSPIRE].

[53] NOvA collaboration, *NOvA: proposal to build a 30 kiloton off-axis detector to study $\nu_\mu \to \nu_e$ oscillations in the NuMI beamline*, `hep-ex/0503053` [InSPIRE].

[54] Daya Bay collaboration, *Observation of electron-antineutrino disappearance at Daya Bay*, *Phys. Rev. Lett.* **108** (2012) 171803 [`arXiv:1203.1669`] [InSPIRE].

[55] RENO collaboration, *Observation of reactor electron antineutrino disappearance in the RENO experiment*, *Phys. Rev. Lett.* **108** (2012) 191802 [`arXiv:1204.0626`] [InSPIRE].

[56] Double CHOOZ collaboration, *Double CHOOZ: a search for the neutrino mixing angle theta(13)*, `hep-ex/0606025` [InSPIRE].

[57] N. Cabibbo, *Time reversal violation in neutrino oscillation*, *Phys. Lett.* **B 72** (1978) 333.

[58] S. Bilenky, J. Hošek and S. Petcov, *On the oscillations of neutrinos with dirac and majorana masses*, *Phys. Lett.* **B 94** (1980) 495.

[59] V.D. Barger, K. Whisnant and R.J.N. Phillips, *CP violation in three neutrino oscillations*, *Phys. Rev. Lett.* **45** (1980) 2084 [InSPIRE].

[60] P.I. Krastev and S.T. Petcov, *Resonance amplification and t violation effects in three neutrino oscillations in the Earth*, *Phys. Lett.* **B 205** (1988) 84 [InSPIRE].

[61] DUNE collaboration, *Long-Baseline Neutrino Facility (LBNF) and Deep Underground Neutrino Experiment (DUNE)*, `arXiv:1512.06148` [InSPIRE].

[62] Hyper-Kamiokande Proto-Collaboration collaboration, *Physics potential of a long-baseline neutrino oscillation experiment using a J-PARC neutrino beam and Hyper-Kamiokande*, *PTEP* **2015** (2015) 053C02 [arXiv:1502.05199] [InSPIRE].

[63] S.M. Bilenky, S. Pascoli and S.T. Petcov, *Majorana neutrinos, neutrino mass spectrum, CP-violation and neutrinoless double beta decay. 1. The Three neutrino mixing case*, *Phys. Rev.* **D 64** (2001) 053010 [hep-ph/0102265] [InSPIRE].

[64] S. Pascoli, S.T. Petcov and L. Wolfenstein, *Searching for the CP-violation associated with Majorana neutrinos*, *Phys. Lett.* **B 524** (2002) 319 [hep-ph/0110287] [InSPIRE].

[65] S. Pascoli, S.T. Petcov and T. Schwetz, *The absolute neutrino mass scale, neutrino mass spectrum, Majorana CP-violation and neutrinoless double-beta decay*, *Nucl. Phys.* **B 734** (2006) 24 [hep-ph/0505226] [InSPIRE].

[66] V. Barger, S.L. Glashow, P. Langacker and D. Marfatia, *No go for detecting CP-violation via neutrinoless double beta decay*, *Phys. Lett.* **B 540** (2002) 247 [hep-ph/0205290] [InSPIRE].

[67] S. Pascoli and S.T. Petcov, *The SNO solar neutrino data, neutrinoless double beta decay and neutrino mass spectrum*, *Phys. Lett.* **B 544** (2002) 239 [hep-ph/0205022] [InSPIRE].

[68] M. Blennow, E. Fernandez-Martinez, J. Lopez-Pavon and J. Menendez, *Neutrinoless double beta decay in seesaw models*, *JHEP* **07** (2010) 096 [arXiv:1005.3240] [InSPIRE].

[69] J.D. Vergados, H. Ejiri and F. Šimkovic, *Neutrinoless double beta decay and neutrino mass*, *Int. J. Mod. Phys.* **E 25** (2016) 1630007 [arXiv:1612.02924] [InSPIRE].

[70] M. Doi et al., *CP violation in Majorana neutrinos*, *Phys. Lett.* **B 102** (1981) 323.

[71] L. Wolfenstein, *CP properties of Majorana neutrinos and double beta decay*, *Phys. Lett.* **B 107** (1981) 7.

[72] S.M. Bilenky, N.P. Nedelcheva and S.T. Petcov, *Some implications of the CP invariance for mixing of Majorana neutrinos*, *Nucl. Phys.* **B 247** (1984) 61 [InSPIRE].

[73] B. Kayser, *CPT, CP and c phases and their effects in Majorana particle processes*, *Phys. Rev.* **D 30** (1984) 1023 [InSPIRE].

[74] KamLAND-Zen collaboration, *Search for Majorana neutrinos near the inverted mass hierarchy region with KamLAND-Zen*, *Phys. Rev. Lett.* **117** (2016) 082503 [arXiv:1605.02889] [InSPIRE].

[75] S. Dell'Oro, S. Marcocci, M. Viel and F. Vissani, *Neutrinoless double beta decay: 2015 review*, *Adv. High Energy Phys.* **2016** (2016) 2162659 [arXiv:1601.07512] [InSPIRE].

[76] S. Blanchet and P. Di Bari, *New aspects of leptogenesis bounds*, *Nucl. Phys.* **B 807** (2009) 155 [arXiv:0807.0743] [InSPIRE].

[77] S. Antusch, S. Blanchet, M. Blennow and E. Fernandez-Martinez, *Non-unitary Leptonic Mixing and Leptogenesis*, *JHEP* **01** (2010) 017 [arXiv:0910.5957] [InSPIRE].

[78] K. Moffat et al., *Three-flavored nonresonant leptogenesis at intermediate scales*, *Phys. Rev.* **D 98** (2018) 015036 [arXiv:1804.05066] [InSPIRE].

[79] Particle Data Group collaboration, *Review of particle physics*, *Chin. Phys.* **C 40** (2016) 100001 [InSPIRE].

[80] Planck collaboration, *Planck 2015 results. XIII. Cosmological parameters*, *Astron. Astrophys.* **594** (2016) A13 [arXiv:1502.01589] [InSPIRE].

[81] A. De Simone and A. Riotto, *On the impact of flavour oscillations in leptogenesis*, *JCAP* **02** (2007) 005 [`hep-ph/0611357`] [ɪɴSPIRE].

[82] S. Blanchet, P. Di Bari and G.G. Raffelt, *Quantum Zeno effect and the impact of flavor in leptogenesis*, *JCAP* **03** (2007) 012 [`hep-ph/0611337`] [ɪɴSPIRE].

[83] S. Biondini et al., *Status of rates and rate equations for thermal leptogenesis*, *Int. J. Mod. Phys.* **A 33** (2018) 1842004 [`arXiv:1711.02864`].

[84] S. Biondini et al., *CP asymmetry in heavy Majorana neutrino decays at finite temperature: the nearly degenerate case*, *JHEP* **03** (2016) 191 [*Erratum ibid.* **08** (2016) 072 [`arXiv:1511.02803`].

[85] S. Biondini, N. Brambilla and A. Vario, *CP asymmetry in heavy Majorana neutrino decays at finite temperature: the hierarchical case*, *JHEP* **09** (2016) 126 [`arXiv:1608.01979`].

[86] S. Blanchet, P. Di Bari, D.A. Jones and L. Marzola, *Leptogenesis with heavy neutrino flavours: from density matrix to Boltzmann equations*, *JCAP* **01** (2013) 041 [`arXiv:1112.4528`] [ɪɴSPIRE].

[87] L. Covi, E. Roulet and F. Vissani, *CP violating decays in leptogenesis scenarios*, *Phys. Lett.* **B 384** (1996) 169 [`hep-ph/9605319`] [ɪɴSPIRE].

[88] A. Fowlie and M.H. Bardsley, *Superplot: a graphical interface for plotting and analysing MultiNest output*, *Eur. Phys. J. Plus* **131** (2016) 391 [`arXiv:1603.00555`] [ɪɴSPIRE].

[89] A. Pilaftsis and T.E.J. Underwood, *Resonant leptogenesis*, *Nucl. Phys.* **B 692** (2004) 303 [`hep-ph/0309342`] [ɪɴSPIRE].

[90] L. Covi and E. Roulet, *Baryogenesis from mixed particle decays*, *Phys. Lett.* **B 399** (1997) 113 [`hep-ph/9611425`] [ɪɴSPIRE].

[91] W. Buchmüller and M. Plümacher, *CP asymmetry in Majorana neutrino decays*, *Phys. Lett.* **B 431** (1998) 354 [`hep-ph/9710460`] [ɪɴSPIRE].

[92] C. Weinheimer, *Direct neutrino mass experiments: Present and future*, *Nucl. Phys. Proc. Suppl.* **118** (2003) 279 [ɪɴSPIRE].

[93] C. Kraus et al., *Final results from phase II of the Mainz neutrino mass search in tritium beta decay*, *Eur. Phys. J.* **C 40** (2005) 447 [`hep-ex/0412056`] [ɪɴSPIRE].

[94] V.M. Lobashev et al., *Direct search for neutrino mass and anomaly in the tritium beta-spectrum: status of 'Troitsk neutrino mass' experiment*, *Nucl. Phys. Proc. Suppl.* **91** (2001) 280 [ɪɴSPIRE].

[95] W. Buchmüller and M. Plümacher, *Spectator processes and baryogenesis*, *Phys. Lett.* **B 511** (2001) 74 [`hep-ph/0104189`] [ɪɴSPIRE].

[96] C.P. Kiessig, M. Plümacher and M.H. Thoma, *Decay of a Yukawa fermion at finite temperature and applications to leptogenesis*, *Phys. Rev.* **D 82** (2010) 036007 [`arXiv:1003.3016`] [ɪɴSPIRE].

[97] G.F. Giudice et al., *Towards a complete theory of thermal leptogenesis in the SM and MSSM*, *Nucl. Phys.* **B 685** (2004) 89 [`hep-ph/0310123`] [ɪɴSPIRE].

[98] A. De Simone and A. Riotto, *Quantum Boltzmann equations and leptogenesis*, *JCAP* **08** (2007) 002 [`hep-ph/0703175`] [ɪɴSPIRE].

[99] M. Beneke et al., *Flavoured leptogenesis in the CTP formalism*, *Nucl. Phys.* **B 843** (2011) 177 [`arXiv:1007.4783`] [ɪɴSPIRE].

[100] A. Anisimov, W. Buchmüller, M. Drewes and S. Mendizabal, *Quantum leptogenesis I*, *Annals Phys.* **326** (2011) 1998 [*Erratum ibid.* **338** (2011) 376] [arXiv:1012.5821] [ɪɴSPIRE].

[101] M. Beneke, B. Garbrecht, M. Herranen and P. Schwaller, *Finite number density corrections to leptogenesis*, *Nucl. Phys.* **B 838** (2010) 1 [arXiv:1002.1326] [ɪɴSPIRE].

[102] T. Frossard, A. Kartavtsev and D. Mitrouskas, *Systematic approach to $\Delta L = 1$ processes in thermal leptogenesis*, *Phys. Rev.* **D 87** (2013) 125006 [arXiv:1304.1719] [ɪɴSPIRE].

[103] E. Nardi, J. Racker and E. Roulet, *CP violation in scatterings, three body processes and the Boltzmann equations for leptogenesis*, *JHEP* **09** (2007) 090 [arXiv:0707.0378] [ɪɴSPIRE].

[104] B. Garbrecht and P. Schwaller, *Spectator Effects during Leptogenesis in the Strong Washout Regime*, *JCAP* **10** (2014) 012 [arXiv:1404.2915] [ɪɴSPIRE].

[105] W. Weckesser, odeintw: *complex and matrix differential equations* (2014).

[106] A.C. Hindmarsh, *ODEPACK, a systematized collection of ODE solvers*, in *Scientific computing*, R.S. Stepleman et al. eds., North-Holland, Amsterdam, Netherlands (1983).

[107] E. Jone et al., SciPy: *open source scientific tools for Python* (2001).

[108] F. Feroz, M. P. Hobson and M. Bridges, *MultiNest: an efficient and robust Bayesian inference tool for cosmology and particle physics*, *Mon. Not. Roy. Astron. Soc.* **398** (2009) 1601 [arXiv:0809.3437].

[109] F. Feroz and M. P. Hobson, *Multimodal nested sampling: an efficient and robust alternative to MCMC methods for astronomical data analysis*, *Mon. Not. Roy. Astron. Soc.* **384** (2008) 449 [arXiv:0704.3704].

[110] F. Feroz, M.P. Hobson, E. Cameron and A.N. Pettitt, *Importance nested sampling and the MultiNest algorithm*, arXiv:1306.2144 [ɪɴSPIRE].

[111] J. Buchner et al., *X-ray spectral modelling of the agn obscuring region in the cdfs: Bayesian model selection and catalogue*, *Astron. Astrophys.* **564** (2014) A125.

[112] C.S. Fong, E. Nardi and A. Riotto, *Leptogenesis in the Universe*, *Adv. High Energy Phys.* **2012** (2012) 158303 [arXiv:1301.3062] [ɪɴSPIRE].

[113] A. Ibarra and G.G. Ross, *Neutrino phenomenology: the case of two right-handed neutrinos*, *Phys. Lett.* **B 591** (2004) 285 [hep-ph/0312138] [ɪɴSPIRE].

[114] S. Antusch, P. Di Bari, D.A. Jones and S.F. King, *Leptogenesis in the two right-handed neutrino model revisited*, *Phys. Rev.* **D 86** (2012) 023516 [arXiv:1107.6002] [ɪɴSPIRE].

[115] S. Blanchet, *Dirac phase leptogenesis*, *J. Phys. Conf. Ser.* **120** (2008) 022007 [arXiv:0710.0570] [ɪɴSPIRE].

[116] S. Lavignac, I. Masina and C.A. Savoy, *Large solar angle and seesaw mechanism: a bottom up perspective*, *Nucl. Phys.* **B 633** (2002) 139 [hep-ph/0202086] [ɪɴSPIRE].